Renewable and Sustainable Energy Reviews 215 (2025) 115636

Contents lists available at ScienceDirect

Renewable and Sustainable Energy Reviews

journal homepage: www.elsevier.com/locate/rser

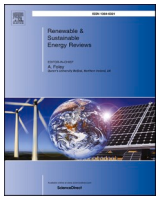

Exploring the role of fracture networks in enhanced geothermal systems: Insights from integrated thermal-hydraulic-mechanical-chemical and wellbore dynamics simulations

Zhenqian Xue [a], Zichao Wei [b], Haoming Ma [c], Zhe Sun [a], Chengang Lu [d], Zhangxin Chen [e,a,f,*]

[a] Department of Chemical & Petroleum Engineering, University of Calgary, Calgary, AB, T2N 1N4, Canada
[b] PetroChina Xinmin Oil Production Plant of Jilin Oilfield Company, Changchun, Jilin, 130000, China
[c] Department of Petroleum and Geosystems Engineering, University of Texas at Austin, Austin, TX, 78712, USA
[d] National Institute of Clean-and-Low-Carbon Energy, Beijing, 102209, China
[e] Ningbo Institute of Digital Twin, Eastern Institute of Technology (tentative), Ningbo, Zhejiang, 315200, China
[f] National Key Laboratory of Petroleum Resources and Engineering, China University of Petroleum (Beijing), Beijing, 102249, China

ARTICLE INFO

Keywords:
Enhanced geothermal system
Thermal-hydraulic-mechanical-chemical model
Discrete fracture network
Vertical-fracture networks
Shear-fracture networks

ABSTRACT

Hot dry rock (HDR) fracturing is a critical stage in the development of enhanced geothermal systems (EGS), and the pattern of an engineered fracture network plays a crucial role in cumulative heat recovery. However, current studies often lack completeness and accuracy when exploring the effects of various fracture networks, overlooking key factors such as chemical reactions, wellbore dynamics, and/or rock mechanical behaviors. This study develops combined thermal-hydraulic-mechanical-chemical (THMC) and wellbore heat loss models, for the first time, to evaluate EGS heat recovery under different vertical-fracture and shear-fracture networks. The results reveal an over 3.9 % variance in heat recovery between THMC and other coupled models, while wellbore heat loss accounts for approximately 7.7 % of the thermal power production, underscoring the significance of incorporating both complex reservoir mechanisms and wellbore heat loss in EGS assessments. In addition, heat recovery improves with increased fracture spacing and number but decreased conductivity. Among vertical-fracture networks, an interrupted complex vertical-fracture system achieves the highest electricity generation of 1119.0 GWh over 20 years of operation. Meanwhile, shear-fracture networks often perform better in heat extraction than vertical-fracture systems, with the case featuring more shear fractures and higher permeability showing the highest electricity output of 1136.7 GWh. Importantly, increasing a fracture number contributes an additional 20.2 GWh, compared to only a 2.2 GWh gain from higher permeability, highlighting the fracture number as the dominant factor in shear-fracture systems. However, due to the higher injection pressure requirements, shear fracturing is best suited for reservoirs with abundant natural fractures. Otherwise, an interrupted complex fracture system is the preferred alternative. This study significantly improves the understanding of EGS performance across different fracture patterns, offering valuable insights to operators for improved decision-making in EGS development.

Abbreviations

EGS	Enhanced geothermal system	TH	Thermal-hydraulic model
HDR	Hot dry rock	THC	Thermal-hydraulic-chemical model
CMG	Computer Modeling Group	THM	Thermal-hydraulic-mechanical model
DFN	Discrete fracture network	THMC	Thermal-hydraulic-mechanical-chemical model

1. Introduction

In addressing the challenge of climate change, geothermal energy emerges as a highly attractive renewable resource with significant

* Corresponding author. Ningbo Institute of Digital Twin, Eastern Institute of Technology (tentative), Ningbo, Zhejiang, 315200, China.
E-mail address: zhachen@ucalgary.ca (Z. Chen).

https://doi.org/10.1016/j.rser.2025.115636
Received 15 October 2024; Received in revised form 16 February 2025; Accepted 15 March 2025

potential to contribute to the clean energy transition. It offers versatility beyond electricity generation, providing solutions for heating, cooling, energy storage, and carbon capture [1]. Among the various geothermal resources, enhanced geothermal systems (EGS) have been widely regarded as the most promising for generating high-capacity, zero-carbon electricity and decarbonizing residential heating and cooling. Many countries recognize the critical role of EGS in the ongoing energy transition. For instance, the United States has emphasized the importance of achieving the goals of the Enhanced Geothermal Shot, a key step toward 100 % carbon-free electricity and net-zero emissions [2].

To extract heat from a hot reservoir with impermeable rock or with natural fractures, such as hot dry rock (HDR) and certain hydrothermal reservoirs [3], it is necessary to conduct an EGS development. To effectively produce heat from HDR and improve heat transmission efficiency, HDR stimulation is essential to create high-conductivity zones that enable commercial fluid flow and heat transfer. Methods such as hydraulic fracturing, thermally-induced fracturing, and chemical stimulation have been successfully employed in the existing EGS projects [4,5]. Table 1 provides a summary of the stimulation technologies currently in use across these projects. Research indicates that hydraulic fracturing, which requires higher breakdown pressures, typically generates simple fracture patterns in HDR reservoirs [6], as shown in Fig. 1A. This method connects injection and production wells by forming primary pathways and may require proppants to keep fractures open [6]. Additionally, CO_2 fracturing, which has been effective in unconventional oil and gas reservoirs [7], shows promise for HDR applications. Although large-scale field operations using CO_2 in HDR reservoirs have not yet been conducted, mesoscale experiments and numerical simulations suggest that CO_2 fracturing could create complex, branched fracture networks in granite [7–10]. In contrast, thermally-induced fracturing, or shear fracturing, exploits thermo-elastic stress to generate more complex fracture paths within an existing fractured reservoir. This is achieved by applying treatment pressure below the minimum principal stress, which reactivates and cleans existing fractures, reopening them without creating new ones (Fig. 1B) [11].

Table 1
Stimulation technologies used in current EGS projects.

Start date	Project	Country	Stimulation methods	Reference
1970	Fenton Hill	United States	Hydraulic fracturing	[12]
1977	Falkenberg	Germany	Hydraulic fracturing	[13]
1978	Le Mayet	France	Hydraulic fracturing with and without proppant	[14]
1987	Soultz	France	Hydraulic fracturing and acidizing	[15]
1982	Rosemanowes	United Kingdom	Hydraulic fracturing	[16]
1984	Hijiori	Japan	Hydraulic fracturing	[17]
1989	Ogachi	Japan	Hydraulic fracturing	[18]
1989	Altheim	Austria	Acidizing and hydraulic fracturing	[19]
1996	Bouillante	France	Thermal-induced stimulation	[20]
2000	Groβ Schönebeck	Germany	Hydraulic gel proppant fracturing	[21]
2001	Berlín	El Salvador	Hydraulic fracturing and chemical stimulation	[22]
2002	Coso	United States	Hydraulic, thermal, and chemical stimulations	[23]
2002	Desert Peak	United States	Shear, chemical, and hydraulic stimulations	[24]
2003	Cooper Basin	Australia	Hydraulic fracturing	[25]
2003	Landau	Germany	Hydraulic fracturing	[26]
2004	Unterhaching	Germany	Chemical stimulation/ acidizing	[27]
2008	Songliao Basin	China	Hydraulic gel proppant fracturing	[28]
2009	Genesys Hannover	Germany	Hydraulic fracturing	[29]
2009	St. Gallen	Switzerland	Chemical and hydraulic stimulations	[30]
2009	Northwest Geysers	United States	Hydraulic fracturing	[31]
2010	Newberry	United States	Hydroshearing and multi-zone isolation techniques	[32]
2010	Pohang	Korea	Hydraulic fracturing	[33]
2011	Mauerstetten	Germany	Chemical and hydraulic stimulations	[34]
2012	Rittershoffen	France	Hydraulic, thermal, and chemical stimulations	[35]
2018	United Downs	United Kindom	Hydraulic fracturing	[36]
2021	Eden	United Kindom	Electrical Reservoir Stimulation	[37]

Geothermal energy extraction from an EGS relies heavily on fracture properties, as fractures serve as the primary channels for heat flow and exchange. Key factors influencing this process include the number of fractures, their spacing, aperture, and permeability. Researchers have also developed complex fracture models to represent CO_2 and shear fracturing-induced fractures in HDR reservoirs, studying correlations between fracture complexity and energy production [38]. However, these models often focus only on fluid flow, heat extraction, or mechanical deformation, using thermal-hydraulic (TH) or thermal-hydraulic-mechanical (THM) approaches. For example, Ma et al. [39] showed that increasing the number of fractures could enhance heat extraction based on TH models, while Slatlem Vik et al. [40] revealed that fracture spacing critically influenced net energy production in a multi-fracture EGS. Aliyu et al. [41] also generated TH modeling and found that variations in fracture permeability played a key role in improving the performance of HDR geothermal reservoirs. THM models have also been used to simplify fracture systems, as seen in Shi et al. [38], who analyzed the effects of fracture network geometries on heat extraction efficiency. Liu et al. [42] evaluated the impact of fracture morphology on EGS performance by considering both continuous and interrupted planar and non-planar fracture schemes, while Liao et al. [43] and Li et al. [44] used discrete fracture network (DFN) models to characterize shear-fracture systems and explore long-term performance.

During EGS development, the injection of a cold fluid alters the pore pressure, reservoir temperature, and stress field as the fluid flows through the rock matrix and fractures, which, in turn, affects the mechanical behavior of a reservoir. In addition to rock deformation due to thermal stress and pore pressure changes, mineral dissolution and precipitation significantly impact heat extraction by modifying fluid pathways. The importance of these mechanisms has been validated in several studies. For instance, Salimzadeh et al. [45] showed that chemical reactions in HDR reservoirs critically affected heat production by comparing THM, thermal-hydraulic-chemical (THC), and thermo-hydraulic-mechanical-chemical (THMC) models. Chen et al. [46] also highlighted the improved estimation accuracy of THMC models, while Song et al. [47] used THMC modeling to demonstrate the distinct contributions of mechanical and chemical mechanisms to reservoir behavior. Gao et al. [48] further evaluated and ranked the importance of different mechanisms on heat extraction performance using THMC models. THMC modeling has also been applied in other aspects of an EGS, such as production comparisons, field optimization, and understanding the influence of various factors on heat production. These include injection temperature, initial reservoir temperature, reservoir permeability [49], injection-induced seismicity, prediction of anthropogenic earthquake occurrence [50], and the optimization of chemical stimulation in fractured geothermal reservoirs [51]. In addition to the complex interactions within a reservoir, heat loss and temperature reduction in wellbores are also crucial for the overall heat recovery of EGS [52]. This is because heat is transferred between the fluids and a formation due to a temperature difference as the fluids move

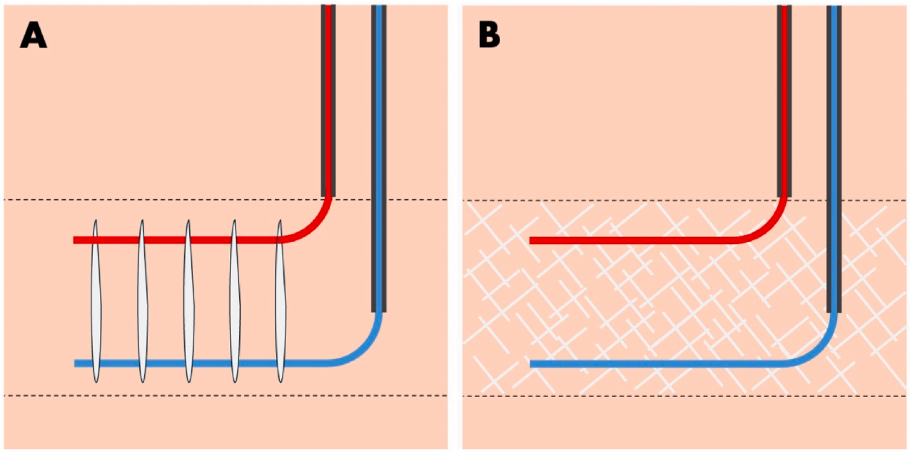

Fig. 1. Conceptual schematics of: (A) a vertical-fracture network and (B) a shear-fracture network (modified from Li et al. [6]).

through a wellbore [53]. For example, Brown et al. [54] found a 7 % difference in thermal power and a 3.4 % temperature difference between a wellhead and its bottom hole in low-temperature geothermal systems. In the case of EGS, a high-temperature geothermal system, it is essential to account for heat loss and temperature drop in the wellbores to accurately predict cumulative heat recovery.

Despite significant advancements, there are still three key limitations in the current investigations of EGS production under different fracture networks, leaving operators with an incomplete understanding. First, there is no study to investigate the impacts of different fracture networks with fully considering thermal, hydraulic, mechanical, and chemical mechanisms. Most studies overlook mechanical or chemical behaviors when assessing the influence of fracture properties on energy production. Given the significant impact of these processes on EGS heat recovery, it is crucial to incorporate all four mechanisms to properly evaluate the effects of different fracture networks. Second, no research has comprehensively investigated EGS heat mining performance in both vertical-fracture and shear-fracture systems. These networks are typically studied separately. Since fracture patterns significantly influence heat recovery and fracture networks can vary under different stimulation methods, this gap leaves operators with an unclear understanding of how various fracture network types affect EGS heat recovery, leading to uncertainty about an optimal fracturing technology to use. Finally, prior studies have primarily focused on reservoir THMC behaviors while neglecting wellbore heat loss, often estimating power and electricity generation based only on subsurface results. Since EGS operations typically occur in deep reservoirs, wellbore heat loss is necessary to be considered for an accurate assessment of cumulative power and electricity production. Therefore, given the significant effects of complex reservoir interactions and wellbore heat loss on EGS heat recovery, it is essential to account for both THMC processes and wellbore heat loss when predicting net power production to ensure more accurate performance assessments.

This study addresses these gaps by developing EGS reservoir models that fully integrate thermal, hydraulic, mechanical, and chemical behaviors while also calculating wellbore heat loss during extraction. First, the complex interactions of thermal, hydraulic, mechanical, and chemical mechanisms are modeled during fluid flow and heat extraction in a reservoir. Then, a wellbore model is employed to calculate temperature drop and heat loss within the wellbores. These reservoir models are used to comprehensively investigate the effects of different fracture networks and the influence of various fracture properties on geothermal energy production, marking a first in this field. Four EGS models, incorporating different mechanisms (i.e., TH, THM, THC, and THMC), are created to evaluate heat extraction performance. The sensitivity of three fracture properties (i.e., fracture spacing, fracture conductivity, and fracture number) is assessed using the developed THMC model. Furthermore, both simple and complex vertical-fracture networks are analyzed to determine their impact on heat recovery. Finally, various shear-fracture systems are modeled using DFN approaches, with their performance evaluated in the context of THMC processes and wellbore heat loss. This comprehensive evaluation not only improves the understanding of the complex underground processes and wellbore heat loss in EGS development but also provides valuable practical guidance for operators in making informed decisions about fracturing technologies and heat recovery strategies.

2. Reservoir Models

In this study, reservoir models are developed using CMG-STARS software, which is a widely recognized and reliable numerical simulator for solving nonlinear systems related to multi-dimensional fluid flow, heat transfer, geomechanical deformation, and chemical reactions in multi-phase, multi-component fluids in porous and fractured media [55–57].

2.1. Mathematical model

To simplify the numerical models, the following reasonable assumptions are made: (1) The formation properties are homogeneous and isotropic [58]; (2) The reservoir is initially saturated with water, and water is the only flow medium, with properties that vary based on temperature and pressure [44]; (3) Local thermal equilibrium is assumed, meaning no temperature difference exists between the fluid and rock at the same location [59]; and (4) Amorphous silica is the primary mineral involved in chemical reactions [60].

The complex interactions of fluid flow, heat transfer, rock deformation, and chemical reactions are critical to the heat mining process in EGS. Additionally, wellbore heat loss, which occurs as fluid is lifted from the downhole to the surface, is essential for accurately predicting geothermal energy recovery. CMG-STARS is used to couple these mechanisms and account for wellbore heat loss.

(1) Fluid flow through the rock matrix and fractures is governed by Darcy's Law. The mass conservation equations for fluid in the matrix and fractures are described by Eqs. (1) and (2) respectively [26].

$$\rho_f S \frac{\partial p}{\partial t} + \nabla \bullet \left(\rho_f \boldsymbol{u}\right) = -\alpha_B \frac{\partial \varepsilon_V}{\partial t} - Q_f \tag{1}$$

$$d_f \rho_f S_f \frac{\partial p}{\partial t} - \nabla_T \bullet \left(d_f \rho_f \boldsymbol{u_f}\right) = -d_f \rho_f \alpha_B \frac{\partial \varepsilon_V}{\partial t} + Q_f \tag{2}$$

Where ρ_f (kg/m^3) is the fluid density; S (Pa^{-1}) is the specific storage of the rock matrix; p (Pa) is the pore pressure; α_B is the Biot coefficient; ε_V is the volumetric strain, calculated as $\varepsilon_V = \varepsilon_{ii} + \varepsilon_{jj} + \varepsilon_{kk}$; Q_f is the mass transfer between the rock matrix and fractures; d_f (m) is the fracture aperture; S_f (Pa^{-1}) is the specific storage of fracture; and $\boldsymbol{u}$ and $\boldsymbol{u_f}$ are Darcy's velocity terms, derived from Eqs. (3) and (4) [61].

$$\boldsymbol{u} = -\frac{k}{\mu_f}\left(\nabla p + \rho_f g \nabla z\right) \tag{3}$$

$$\boldsymbol{u_f} = -\frac{k_f}{\mu_f}\left(\nabla_T p + \rho_f g \nabla z\right) \tag{4}$$

Where k (m^2) is the matrix permeability; μ_f (Pa • s) is the fluid viscosity; and k_f (m^2) represents the fracture permeability.

(2) Thermal equilibrium transport is assumed between the solid and the fluid, meaning the temperatures of both are equal at any point in space and time. The energy conservation equations for the porous media and fractures are expressed as Eqs. (5) and (6) respectively [42].

$$\left(\rho C_p\right)_{eff}\frac{\partial T}{\partial t} + \rho_f C_{p,f}\boldsymbol{u} \bullet \nabla T - \nabla \bullet \left(\lambda_{eff}\nabla T\right) = -Q_{f,E} \tag{5}$$

$$d_f\left(\rho C_p\right)_{eff}\frac{\partial T}{\partial t} + d_f\rho_f C_{p,f}\boldsymbol{u_f} \bullet \nabla_T T - \nabla_T \bullet \left(d_f\lambda_{eff}\nabla T\right) = Q_{f,E} \tag{6}$$

Where $\left(\rho C_p\right)_{eff}$ is the effective volumetric capacity and is calculated by $\left(\rho C_p\right)_{eff} = (1-\phi)\rho_s C_{p,s} + \phi\rho_f C_{p,f}$, where ρ_s (kg/m^3) is the solid density and $C_{p,s}$ (J/(kg • K)) is the specific heat of the solid; T (K) is the temperature; $C_{p,f}$ (J/(kg • K)) is the specific heat of the fluid; λ_{eff} (W/(m • K)) is the effective thermal conductivity and can be calculated by $\lambda_{eff} = (1-\phi)\lambda_s + \phi\lambda_f$, where λ_s and λ_f are the thermal conductivities of the solid and fluid respectively; $Q_{f,E}$ represents the heat transfer between the porous media and fractures.

(3) Based on the law of linear elasticity, the constitutive relations of a poroelastic medium can be expressed in terms of the stress σ_{ij}, strain ε_{ij}, pore pressure p, and temperature T. The stress equilibrium equation in rocks is given by Ref. [62]:

$$\sigma_{i,j} = 2G\varepsilon_{ij} + \frac{2G\nu}{1-2\nu}\varepsilon_{kk}\delta_{ij} - \alpha_B p\delta_{i,j} - K\alpha_T T\delta_{i,j} \tag{7}$$

Where ν is the Poisson's ratio; G (Pa) and K (Pa) are the shear modulus and the bulk modulus, expressed in terms of Young's modulus E (Pa) as: $G = E/[2(1+\nu)]$ and $K = 3/[(1-2\nu)]$; δ_{ij} is the Kronecker symbol, which is equal to 1 when $i = j$ and 0 when $i \neq j$; α_B is the Biot coefficient; and α_T (K^{-1}) is the volumetric thermal expansion coefficient. The correlations between displacement and strain are expressed as $\varepsilon_{ij} = \left(u_{i,j} + u_{j,i}\right)/2$, and the equilibrium equation is $\sigma_{ij,i} + F_i = 0$, where u_i (m) is the displacement and F_i (N/m^3) is the body force per unit volume. Therefore, the rock deformation equation can be derived as [63]:

$$Gu_{i,jj} + \frac{G}{1-2\nu}u_{j,ji} - \alpha_B p_{,i} - K\alpha_T T_{,i} + F_i = 0 \tag{8}$$

Where the third term in this equation accounts for changes in pore pressure, and the fourth term represents thermal stress induced by the temperature variations.

(4) Quartz, being the major component in granite rock reservoirs, is assumed to be the primary mineral involved in chemical reactions for this study. The relevant solid or mineral reaction is: $SiO_{2(s)} + 2H_2O \leftrightarrow H_4SiO_4$. The reaction rate during water circulation is temperature-dependent and can be determined by Ref. [64]:

$$R = A_n k_n a_{H^+}\left(\frac{Q_n}{K_n} - 1\right) \tag{9}$$

Where A_n (m^2/m^3) is the reactive surface area; k_n is the standard rate constant; a_{H^+} is the activity of H^+; Q_n is the concentration product of fluid species participating in the reaction; K_n is the solubility product constraint for the reaction. If $Q_n/K_n > 1$, precipitation occurs, and if $Q_n/K_n < 1$, dissolution occurs. The standard rate constant is given by Ref. [65]:

$$k_n = k_{ref} \bullet exp\left[-\frac{E}{R}\left(\frac{1}{T} - \frac{1}{T_0}\right)\right] \tag{10}$$

Where k_{ref} is the rate constant at the reference temperature (298.15 K); E is the activation energy; R is the universal gas constant; T is the absolute temperature; and T_0 is the reference temperature (298.15 K). The solute transportation in the rock matrix and fractures is described by Eqs. (11) and (12) respectively [47].

$$\frac{\partial\left(\phi\rho_f C_f\right)}{\partial t} + \nabla \bullet \left(\boldsymbol{u}\rho_f C_f\right) - \nabla \bullet \left(\phi\rho_f D_{eff,m}\nabla C_f\right) = 0 \tag{11}$$

$$d_f\frac{\partial\left(\phi_f\rho_f C_f\right)}{\partial t} + d_f\nabla_T \bullet \left(\boldsymbol{u_f}\rho_f C_f\right) - \nabla_T \bullet \left(d_f\phi_f\rho_f D_{eff,f}\nabla C_f\right) = \Delta R + Q \tag{12}$$

Where ϕ and ϕ_f are the porosities of the matrix and fracture; $D_{eff,m}$ and $D_{eff,f}$ are the effective mass diffusion coefficients in the matrix and fracture; Q is the solute flux from the matrix to the fracture.

(5) Porosity changes in response to both mechanical deformation and chemical reactions. In the case of rock deformation, porosity is influenced by pressure, temperature, and total mean stress. The variation in porosity due to rock deformation can be calculated by Ref. [66]:

$$\phi^{n+1} = \phi^n + (c_0 + c_2a_1)\Delta P + (c_1 + c_2a_2)\Delta T \tag{13}$$

$$\begin{cases} c_0 = \dfrac{1}{V_b^0}\left(\dfrac{dV_p}{dp} + V_b\alpha_B c_b\dfrac{d\sigma_m}{dp} - V_p\alpha_T\dfrac{dT}{dp}\right) \\ c_1 = \dfrac{V_p}{V_b^0}\alpha_T \\ c_2 = -\dfrac{V_b}{V_b^0}\alpha_B c_b \\ a_1 = factor\left\{\dfrac{2}{9}\dfrac{E}{1-\nu}\alpha_B c_b\right\} \\ a_2 = factor\left\{\dfrac{2}{9}\dfrac{E}{1-\nu}\alpha_T\right\} \end{cases}$$

Where V_b (m^3) is the bulk volume; V_p (m^3) is the pore volume; c_b (Pa^{-1}) is the bulk compressibility; σ_m (Pa) is the mean total stress. In the case of chemical reactions, the change in porosity due to dissolution or precipitation can be calculated by the total volume fraction change as [46]:

$$\Delta\phi_c = 1 - (f_m - f_u) - V_{ini-m}/V_{medium} \tag{14}$$

Where f_m is the total mineral volume fraction $(V_{mineral}/V_{medium})$; f_u is the non-reactive mineral fraction. Therefore, the current porosity during the operation can be calculated as: $\phi = \phi^{n+1} + \Delta\phi_c$. The permeability variation with evolving porosity can be represented by Ref. [60]:

$$\frac{k}{k_0} = \left(\frac{\phi}{\phi_0}\right)^n\left(\frac{1-\phi_0}{1-\phi}\right)^2 \tag{15}$$

Where k (m^2) is the current permeability; k_0 (m^2) is the initial permeability; ϕ_0 is the initial porosity; and n is an exponent value representing the sensitivity of permeability to porosity changes.

(6) Wellbore dynamics during geothermal operations is analyzed by using the Semi-Analytical Model (SAM) in CMG-STARS, specifically addressing enthalpy changes, pressure drops, and heat loss from the wellbore as fluid is transported from the downhole to the surface. The pressure drop in the wellbore is influenced by factors such as friction, gravity, and kinetic energy, which is expressed by Ref. [67]:

$$\frac{dP}{dz} = \rho_f g - \rho_f u_f \frac{du_f}{dz} - f\frac{\rho_f {u_f}^2}{2r_{in}} \tag{16}$$

Where P (Pa) is the fluid pressure in the wellbore; z is the wellbore depth; u_f is the fluid velocity in the wellbore; f is the friction factor (determined by Colebrook's equation); r_{in} (m) is the inner diameter of the wellbore. The radial heat loss from the wellbore to the surrounding formation is described by Ref. [67]:

$$Q_{loss} = 2\pi r_{to} U_t \left(T_f - T_{wb}\right) \tag{17}$$

Where T_f is the fluid temperature inside the tubing; T_{wb} is the temperature at the cementing/formation interface; U_{to} is the overall heat transfer coefficient, and can be determined by Ref. [67]:

$$\frac{1}{U_t} = \frac{r_{to}}{r_{ti}h_f} + \frac{r_{to}\ln\left(r_{to}/r_{ti}\right)}{k_t} + \frac{r_{to}\ln\left(r_{ins}/r_{to}\right)}{k_{ins}} + \frac{r_{to}}{r_{ins}(h_c + h_r)} + \frac{r_{to}\ln\left(r_{co}/r_{ci}\right)}{k_{cas}} + \frac{r_{to}\ln\left(r_{wb}/r_{co}\right)}{k_{cem}} \tag{18}$$

Where r_{to}, r_{ti}, r_{ins}, r_{co}, r_{ci}, and r_{wb} are the radius of the outer tubing, inner tubing, outer insulation interface, outer casing, inner casing, and cementing/formation interface, respectively; h_f is the fluid convective heat transfer coefficient; h_c is the fluid convective heat transfer coefficient in the annulus; h_r is the radiative heat transfer coefficient of fluid in the annulus; k_t, k_{ins}, k_{cas}, and k_{cem} are the thermal conductivities of the tubing, insulation, casing, and cementing, separately.

2.2. Model description

The reservoir models created in this study are based on our previous models of the Qiabuqia EGS [61–64,68,69]. The Qiabuqia field is recognized as a promising case for EGS numerical simulations, and its detailed characteristics are documented in previous studies [58,70]. A base model is first developed to represent an area of 1500 × 1500 × 3800 m^3 with a total of 34,200 grid blocks. The key reservoir properties of this model can be found in Table 2.

In this model, three horizontal wells are drilled, including one injector (GR1) and two producers (PR1 and PR2). The well spacing is set at 500 m, and the wells are drilled at a depth of 3700 m, where the highest downhole temperature has been recorded [71]. The horizontal length of each well is 750 m. The stimulation method assumed in the base model is a multi-stage hydraulic fracturing of the injection well. This creates a simple vertical-fracture network with six planar fractures, each located at a depth of 3700 m. The fractures have a spacing of 150 m, a half-length of 500 m, and a conductivity of 10 mDm, connecting the injection and production wells. To ensure accurate calculations, the grid resolution in the enhanced reservoir is refined five times horizontally and three times vertically. A grid refinement study is conducted by halving the grid block dimensions and reducing them by a third in all directions. The results show variations of less than 0.2 %, indicating that the original grid is sufficiently resolved. Fig. 2 provides a schematic diagram of this base model.

Table 2
Parameter setting of the base reservoir mode.

Parameter	Value	Parameter	Value
Reservoir properties		Well spacing, m	500
Granite density, kg/m^3	2623	Well horizontal section length, m	750
Porosity, %	2.49	Inner and outer tubing radius, m	0.15, 0.18
Temperature, °C	25–0.057z	Insulation radius, m	0.2
Pressure, MPa	0.1-0.01z	Inner and outer casing radius, m	0.24, 0.3
Temperature at 3700m subsurface, °C	236	Tubing thermal conductivity, W/ (m • °C)	32.29
Pressure at 3700m subsurface, MPa	37	Insulation thermal conductivity, W/ (m • °C)	0.06
Horizontal permeability, mD	0.26	Casing thermal conductivity, W/ (m • °C)	32.29
Vertical permeability, mD	0.026	Cement thermal conductivity, W/ (m • °C)	0.26
Granite heat conductivity, W/ (m • °C)	3.0		
Granite specific heat, J/ (kg • °C)	980	***Engineered fracture properties***	
Thermal expansion coefficient ($°C^{-1}$)	7.5×10^{-6}	Fracture spacing, m	150
Biot's coefficient	0.7	Fracture half-length, m	500
Young's modulus (GPa)	44.1	Fracture conductivity, mDm	10
Poisson's ratio	0.23	Fracture number	6
Silica initial volume fraction	0.45		
Horizontal natural fracture spacing, m	10	***Operating properties***	
Vertical natural fracture spacing, m	10	Injection rate, kg/s	45
		Injection temperature, °C	40
Wellbore properties		Production pressure, MPa	37
Well depth, m	3700	Operation time, year	20

For the boundary conditions, fluid flow is restricted at both the top and bottom boundaries of the model. The temperature at the bottom boundary is set based on the temperature distribution observed in the Qiabuqia field. At the top boundary, a heat loss model is implemented to simulate the heat losses from the surface to the atmosphere. For the initial conditions, based on the exploration data from this field, the temperature and pressure at the top of the study area are set to 236 °C and 37.1 MPa, respectively.

The wellbore model is configured by dividing the vertical section of each well into 150 equal segments. The lengths of the casing and insulation are both set to match the wellbore depth of 3700 m. Detailed parameter settings of the wellbore model can be found in Table 2. Water is used as the heat transmission fluid in this work, and a water stream at 40 °C is injected into the reservoir through the injection well. The operational constraints for the wells are as follows: the injection well operates at a constant rate of 45 kg/s, and the production wells maintain a constant pressure of 37 MPa. The system is designed for heat extraction and water circulation over a 20-year period, which can represent the potential for the heat extraction of the Qiabuqia geothermal field [58,70,73]. Detailed settings of the operating parameters for the simulation are outlined in Table 2.

2.3. Investigated scenarios

This study initially investigates the impact of different coupling mechanisms on reservoir performance and geothermal energy recovery by developing four models: TH, THM, THC, and THMC. Each model represents a different combination of physical processes. The TH model considers only fluid flow and heat transfer within the matrix and fractures during reservoir development. The THM model adds rock deformation to the fluid flow and heat transfer. The THC model accounts for fluid flow, heat transfer, and chemical reactions during heat extraction.

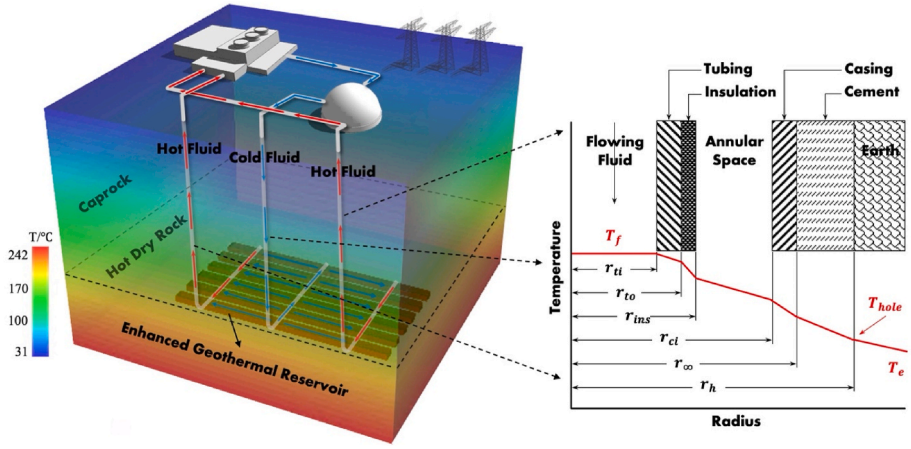

Fig. 2. Schematic diagrams of: (left) a horizontal-well-EGS numerical model, and (right) a wellbore structure showing potential temperature loss (modified from Chong et al. [72]).

Finally, the THMC model fully couples fluid flow, heat transfer, mechanical deformation, and chemical reactions during water circulation and energy production. The wellbore heat loss is considered in all of these models.

In addition, the study examines the effects of various fracture properties, including fracture spacing, number, and conductivity, on heat extraction performance. The fracture spacing is varied from 50 to 200 m, fracture number from 5 to 14, and fracture conductivity from 5 to 20 mDm to assess their sensitivity. In this analysis, the fracture pattern is assumed to consist of continuous, simple vertical fractures. To ensure effective connectivity between injection and production wells, the fracture half-length is set equal to the well spacing (500 m). Details of the parameters used in the sensitivity analysis are provided in Table 3.

Previous studies have demonstrated that hydraulic fracturing in granite rock typically creates simple fracture networks, while CO2 fracturing is more likely to result in complex fracture systems. To simplify the representation of different fracturing methods, various fracture networks are modeled, as shown in Fig. 3. Scenario 3-1 involves only primary fractures (half-length: 500 m) created through the injector to connect the injector and producers. Scenario 3-2 incorporates both the primary and secondary fractures with a 500 m half-length for primary fractures and a 50 m length for secondary fractures. Scenarios 3-3 and 3–4 represent interrupted simple and complex fracture networks generated from the injecter and producers, respectively. The half-length of primary fractures is 250 m and the length of secondary fractures in the complex fracture network is 50 m.

Furthermore, the discrete fracture network (DFN) method is utilized to characterize fracture systems generated by shear fracturing, where pre-existing natural fractures are cleaned and re-opened. Since the study focuses on the impact of different fracture patterns on EGS heat recovery, the shear-fracture networks are randomly generated using Petrel software. As shown in Fig. 4, four different fracture networks with varying complexity and permeability are considered. Scenarios 4-1 and 4-2 feature 135 shear fractures with average permeabilities of 300 mD and 600 mD, respectively. Scenarios 4-3 and 4-4 represent shear-fracture systems with 35 fractures and average permeabilities of 300 mD and 600 mD, respectively.

Table 3
Parameter setting for the sensitivity analysis of various fracture properties.

Parameters	Values
Fracture spacing (FS), m	50/100/150/200
Fracture number (FN)	5/8/11/14
Fracture conductivity (FC), mDm	5/10/15/20

2.4. Computational indicators

Two key indicators are used to evaluate the heat extraction performance of EGS, including the temperature of the produced fluid at the surface and the amount of geothermal electricity generated. The surface production temperature is directly calculated using CMG-STARS, while generated geothermal electricity (E) is determined by the installed geothermal power capacity (W_p), which is defined as [70]:

$$W_p = 0.3 \bullet Q \bullet \Delta H \bullet (1 - T_{in} / T_{out}) \tag{19}$$

Where Q (kg/s) is the fluid production rate in the whole system, ΔH (J/kg) is the enthalpy change between injected enthalpy and produced enthalpy; T_{in} (K) is the rejection temperature; T_{out} (K) is the average temperature at the production wells. In this study, it is assumed that the produced heat is fully utilized for power generation, with an energy conversion efficiency of 30 %, meaning 30 % of the thermal energy is converted into geothermal electricity. To assess the reliability of the geothermal power plant, a capacity factor of 0.7 is used. This allows for the calculation of cumulative geothermal electricity generation as [74]:

$$E = \sum_{t}^{T} W_p^t \bullet H_{annual} \bullet 0.7 \tag{20}$$

Where T is the total number of operation periods, and H_{annual} represents the total annual hours, which equals 8760 (365 days × 24 h).

3. Results

This section presents the detailed heat extraction performance of various coupling models. It also analyzes the sensitivities of fracture spacing, number, and conductivity, as well as the impact of different fracture networks on geothermal energy recovery. Additionally, the heat extraction efficiency of thermally induced fracture systems is demonstrated.

3.1. EGS performance in different coupling models

Fig. 5 shows the EGS performance of different coupling models. The results indicate that the THM model has the lowest surface production temperature (202.5 °C) compared to the TH model (203.2 °C), while the THC (204.9 °C) and THMC (204.1 °C) models show higher temperatures. These variations can be attributed to changes in porosity, as shown in Fig. 6. Specifically, the THM model shows increased porosity along the flow path due to mechanical deformation, which lowers injection pressures and reduces injection-production pressure differences

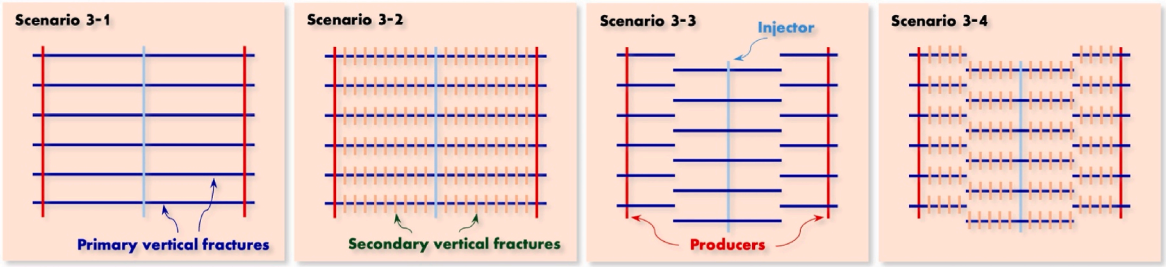

Fig. 3. Upward geometric views of various vertical-fracture networks.

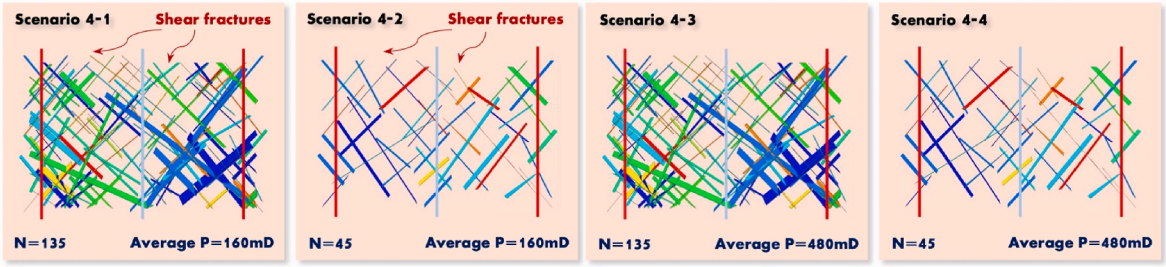

Fig. 4. Upward geometric views of various shear-fracture networks.

(Fig. 5c). Despite the decreased water production rate (Fig. 5d), the enhanced reservoir flowability allows cold fluid to reach the producers faster, leading to a more rapid decline in production temperature. As a result, the THM model generates the lowest electricity output (917.6 GWh).

In the THC model, the dissolution of silica minerals improves conductivity near the wellbore, increasing the residence time of cold injected fluid in the reservoir and reducing the injection-production pressure difference. Consequently, the water production rate and surface production temperature are higher, leading to increased electricity production (1039.0 GWh) compared to the TH model (935.9 GWh). Although the THC model creates a larger high-conductivity area, it requires higher injection pressure and results in a greater injection-production pressure difference than the THM model, which generates a longer but narrower high-conductivity region.

The THMC model, which integrates both mechanical deformation and chemical reactions, benefits from extended fluid flow and lower injection pressures. This leads to a higher surface production temperature and increased water production rates, contributing to greater electricity generation (1001.1 GWh) compared to the TH (935.9 GWh) model. However, the THMC model produces less electricity than the THC model (1039.0 GWh) but more than the THM model (917.6 GWh). Although surface production temperatures among the models exhibit small variations, differences in production rates are more significant due to the various mechanisms involved. This results in an approximately 9.9 % difference in electricity generation between the THMC and TH models, and differences of 3.6 % and 11.7 % when comparing the THMC model with the THM and THC models. These findings highlight the importance of incorporating heat transfer, fluid flow, geomechanics, and geochemistry when evaluating EGS heat extraction performance.

The THM, THC, and THMC models in this work are based on our previously validated Qiabuqia TH model [75,76]. Since no prior studies have examined different coupling models for the Qiabuqia geothermal field, model validation was performed by comparing results with previous research. The results show that key parameters (e.g., porosity, produced fluid temperature, and generated power and electricity) show trends consistent with previous studies, confirming model accuracy. Specifically, the THC model presents increased porosity near the wellbore, the THM model shows an increase along the flow path, and both the THM and THMC models exhibit similar variations, aligning with prior research [45,60]. Additionally, the opposing effects of mechanical deformation and chemical reactions on production temperature and heat recovery are consistent with previous findings [45,60]. These consistencies validate the accuracy of the coupled THM, THC, and THMC models generated in this work, demonstrating that the THMC model reliably predicts complex reservoir interactions during EGS development.

Temperature drop in wellbores across all models is most significant during the early stages of development, gradually decreasing over time and stabilizing in the later years. This occurs because the initially produced fluid, which is warmer than the surrounding formation, transfers heat to the formation until thermal equilibrium is reached. In addition, higher flow rates carry more enthalpy and geothermal energy, enhancing heat transfer and reducing the temperature difference between the wellbore and the surrounding formation [77]. Consequently, the THC model exhibits the smallest temperature loss in wellbores due to its higher water production rate, while the THM model experiences the largest temperature loss. By the end of the 20-year operation, all models demonstrate similar overall heat loss, as indicated by comparable temperature drops. Specifically, heat loss in the TH model is −134.9 W/m, while the THM, THC, and THMC models exhibit heat losses of −137.2 W/m, −134.6 W/m, and −136.5 W/m, respectively. However, these wellbore heat losses represent 7.8 %, 7.5 %, 7.8 %, and 7.6 % of the thermal power recorded at the surface, underscoring the necessity of considering wellbore heat loss in EGS development. Therefore, the coupled THMC and wellbore dynamics model developed in this study is reliable for investigating EGS heat recovery across different fracture networks.

3.2. *EGS performance under different fracture properties*

Fig. 7 demonstrates the effect of varying fracture spacings on EGS performance. The results show that surface production temperature (Fig. 7a), geothermal power output, and electricity generation (Fig. 7b) all increase as fracture spacing widens, but the rate of improvement decreases at larger spacings. For instance, electricity generation rises from 862.2 GWh to 975.3 GWh when fracture spacing expands from 50 m to 100 m, a 13.1 % increase. However, this growth slows to 2.6 % as

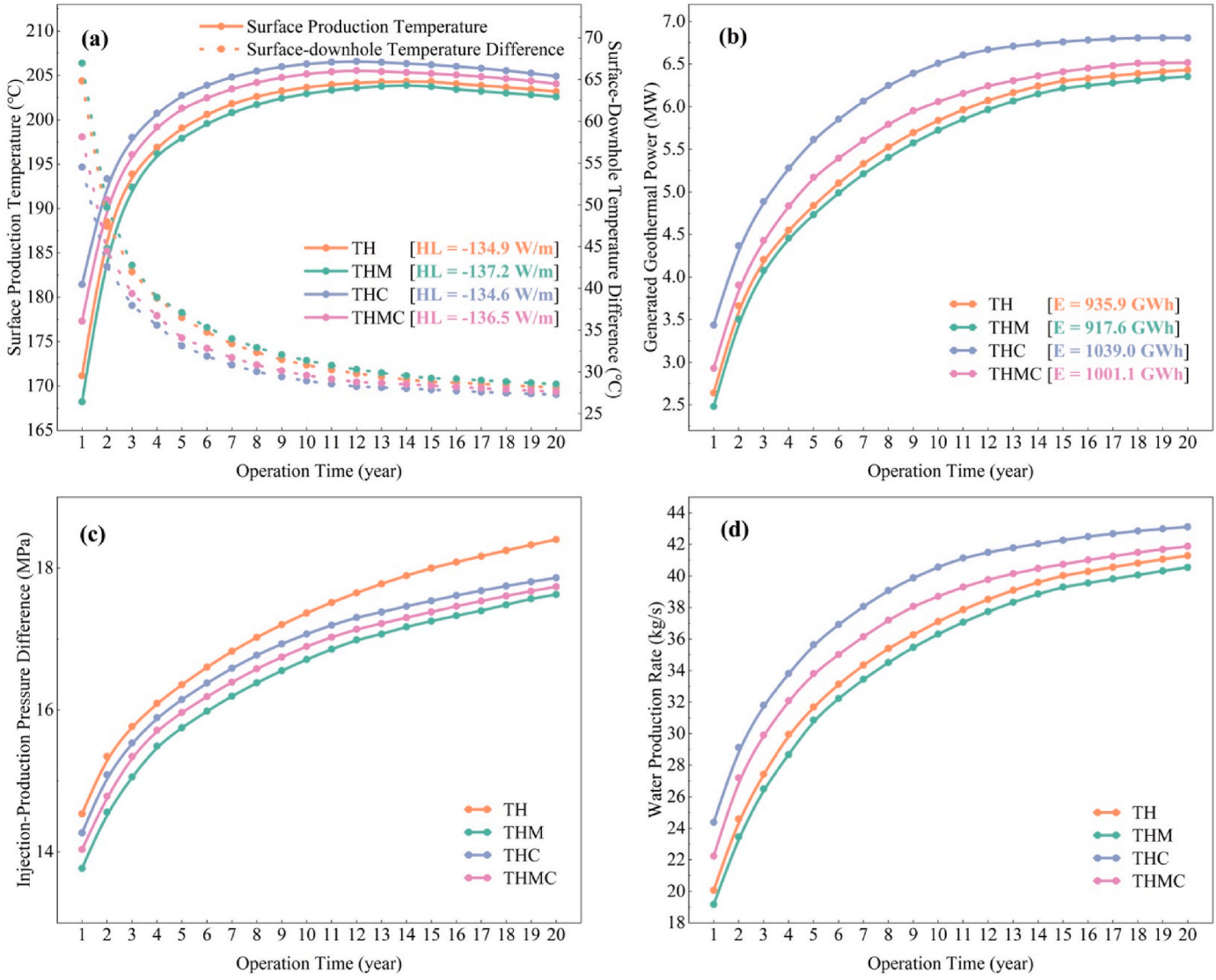

Fig. 5. EGS performance of different coupling models: (a) surface production temperature and temperature loss within wellbores; (b) geothermal power and electricity generation; (c) injection-production pressure difference; and (d) water production rate.

the spacing grows from 100 m to 150 m and further drops to 0.6 % at 200 m. Meanwhile, wider fracture spacing leads to higher peak surface production temperature increases and delays thermal breakthrough. When spacing increases from 50 m to 100 m, the peak production temperature increases from 196 °C to 204 °C, and the thermal breakthrough is delayed from year 4 to year 10. This trend is attributed to fracture interference and heat extraction area size. Narrower fracture spacing intensifies fracture interference and limits the heat extraction area, leading to higher injection pressures and slower fluid flow to the production wells. Consequently, at a 50 m spacing, the injection-production pressure difference is highest (Fig. 7c), the water production rate is lowest (Fig. 7d), and the surface production temperature is the lowest, leading to reduced power and electricity outputs. Regarding heat loss in wellbores, all scenarios exhibit a gradual decline due to the decreasing temperature difference between the produced fluid and the surrounding formation over time. However, as the fracture spacing increases, higher production rates lead to greater overall heat loss. The highest heat loss (−137.1 W/m) occurs at 200 m spacing, while the lowest (−121.3 W/m) is observed at 50 m spacing.

Fig. 8 shows the performance of EGS models with varying numbers of fractures. The results indicate that increasing the number of fractures leads to higher surface production temperatures (Fig. 8a), increased power generation, and greater electricity production (Fig. 8b). With the same fracture spacing, additional fractures expand the heat extraction area, lowering the required injection pressure (Fig. 8c) and increasing water production rates (Fig. 8d). This larger heat extraction area also delays the intrusion of cold fluid into fractures, slowing the decline in surface production temperature. The combination of higher water production rates and elevated outlet temperatures enhances heat extraction. Consequently, the case with 14 fractures achieves the highest electricity output (1079.1 GWh), while the case with 5 fractures yields the lowest (940.2 GWh). However, as the number of fractures increases further, the improvement in heat recovery diminishes. Regarding wellbore heat loss, scenarios with more fractures initially experience smaller temperature losses due to higher water mass flow rates. The greater enthalpy and geothermal energy carried by the fluid reduce the temperature difference between the wellbore and the surrounding formation. Over time, as the hot fluid flows through the wellbore and the temperature difference between the wellbore and the formation decreases, these cases present similar temperature drops (27.5 °C). However, greater overall wellbore heat losses are observed in cases with more fractures due to higher production rates (FN14: −138.5 W/m vs. FN5: −131.4 W/m).

Fig. 9 presents the EGS performance across models with different

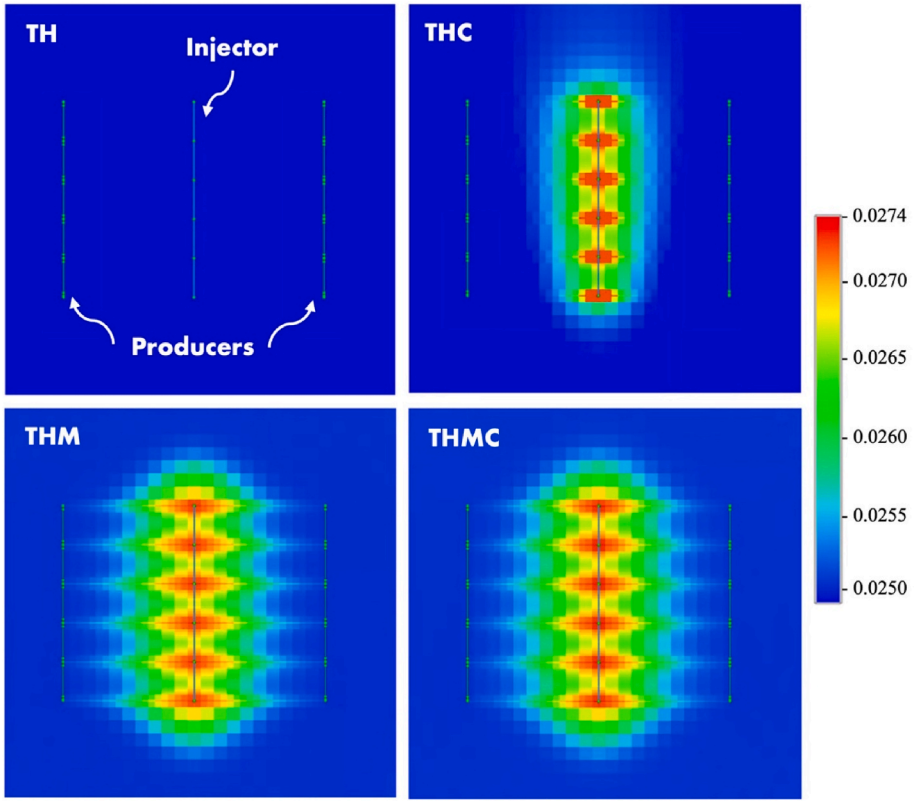

Fig. 6. Porosity distributions after a 20-year operation in various coupling models.

fracture conductivities. The results show that as fracture conductivity increases, surface production temperature, power output, and electricity production all decrease (Fig. 9a and b). Specifically, a fracture conductivity of 5 mDm achieves the largest electricity production at 983.7 GWh, while a conductivity of 20 mDm results in the lowest output of 939.7 GWh. Fracture conductivity, governed by fracture permeability and aperture, affects fluid flow behavior. Higher conductivity facilitates the movement of injected fluid into the production wells, accelerating the decline in outlet production temperature and increasing water production rates (Fig. 9d). However, as shown in Fig. 9c, under fixed injection rate and production pressure, greater conductivity also lowers injection pressure, reducing injection-production pressure differences (5mDm: 22 MPa vs. 20mDm: 15 MPa). While higher conductivity improves reservoir flowability, its effect on water production is counterbalanced by the reduced pressure difference. As a result, higher conductivity cases exhibit increased production rates and lower wellbore heat losses (20mDm: −130.4 W/m vs. 5mDm: −134.9 W/m). In summary, although greater conductivity enhances flowability, it negatively impacts power and electricity generation. Meanwhile, the higher injection pressure required for low-conductivity cases poses operational challenges. Therefore, determining an optimal fracture conductivity is essential for balancing reservoir performance and operational feasibility.

3.3. EGS performance under different vertical-fracture networks

Fig. 10 demonstrates the EGS performance across models with various vertical-fracture networks. The results show that these cases bring the consistent trends in surface production temperature and heat recovery across these cases, with the following ranking: Scenario 3–4 (205.1 °C; 1119.0 GWh) > Scenario 3-3 (202.5 °C; 1050.8 GWh) > Scenario 3-2 (200.2 °C; 1016.6 GWh) > Scenario 3-1 (198.4 °C; 975.3 GWh).

When comparing continuous simple and complex vertical fractures (Scenario 3-1 vs. Scenario 3-2), Scenario 3-2 achieves a higher surface production temperature due to the presence of secondary fractures. These fractures expand the fluid-rock contact area, diverting cold injected fluid and slowing its movement toward production wells. Additionally, the larger stimulated area in Scenario 3-2 reduces the injection pressure required to maintain the same fluid injection rate, leading to a smaller injection-production pressure difference (Fig. 10c). This also improves flow characteristics, resulting in a higher water production rate (Fig. 10d) and slightly smaller heat loss in the wellbore compared to Scenario 3-1 (Scenario 3-2: −132.1 W/m vs. Scenario 3-1: −133.1 W/m). Similarly, in interrupted simple and complex vertical-fracture networks (Scenario 3-3 vs. Scenario 3–4), Scenario 3–4 outperforms Scenario 3-3 due to branch fractures. Scenario 3–4 exhibits higher surface production temperatures, reduced heat loss in the wellbores (Fig. 10a), higher water production rates (Fig. 10d), and a smaller injection-production pressure difference (Fig. 10c), leading to greater net power and electricity generation. Notably, the presence of secondary fractures effectively enhances fluid injectivity, resulting in an average reduction of 5 MPa in the injection-production pressure difference, which is favorable for field operations.

When comparing continuous and interrupted vertical-fracture networks (scenarios 3-1/3-2 vs. scenarios 3-3/3-4), the higher surface production temperatures in interrupted networks can be explained by the absence of a direct high-conductivity pathway for fluid flow. In these networks, injected cold fluid takes longer to reach the production wells, slowing the decline in surface production temperature over time compared to continuous networks. Consequently, interrupted vertical-fracture networks exhibit more stable geothermal power production. Although injecting the same volume of water into interrupted fracture networks requires higher injection pressures (Fig. 10c), which presents greater operational challenges, the complex fracture system in interrupted networks helps mitigate the increased pressure requirement. For example, the injection-production pressure difference increases from 19 MPa in the continuous simple-fracture pattern (scenarios 3-1) to 24 MPa

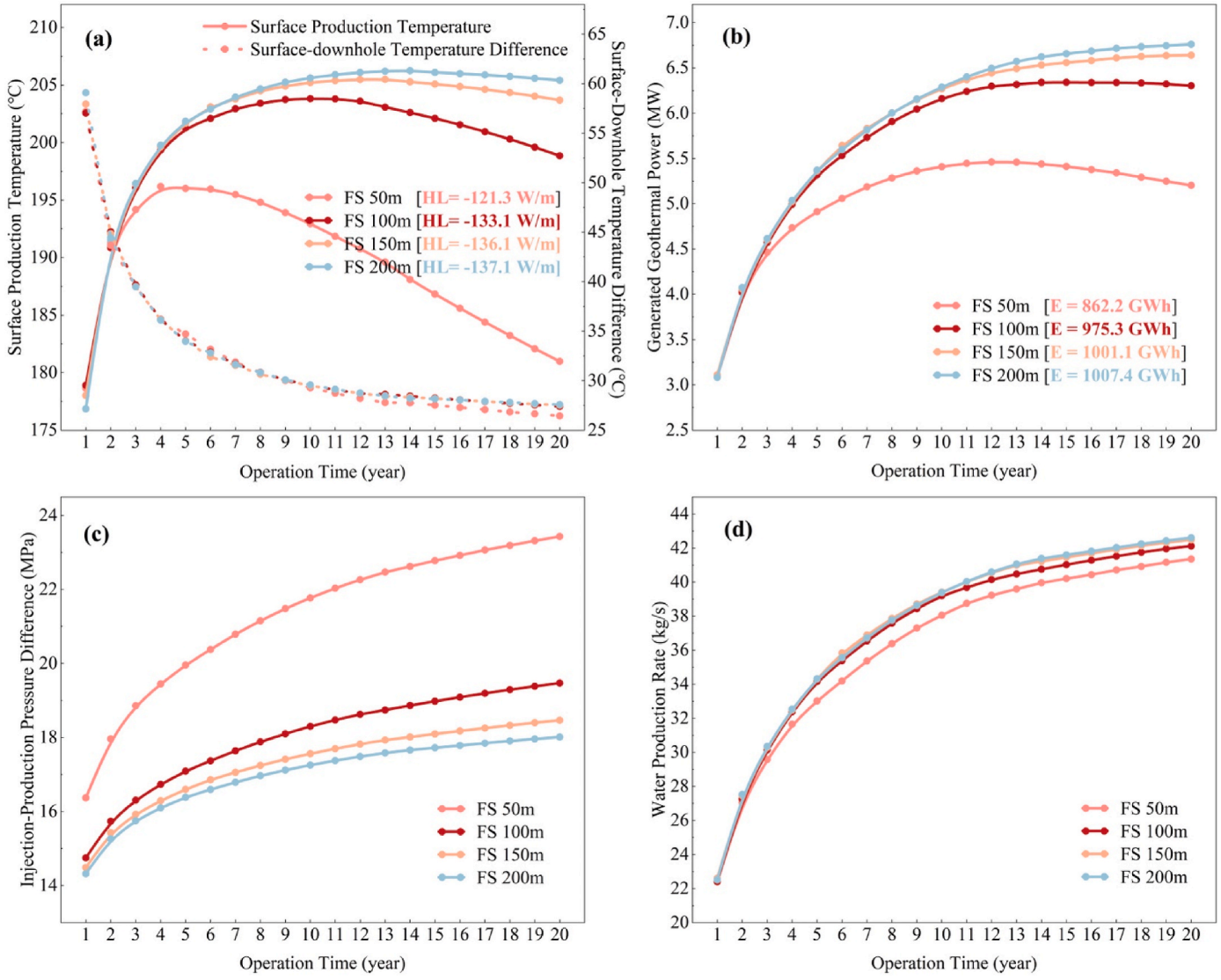

Fig. 7. EGS performance of models with different fracture spacing: (a) surface production temperature and temperature loss within wellbores; (b) geothermal power and electricity generation; (c) injection-production pressure difference; and (d) water production rate.

in the interrupted simple-fracture pattern (scenarios 3-3). However, in complex-fracture systems, this increase is smaller, with the pressure difference rising by 3 MPa from the continuous complex-fracture pattern (scenarios 3-3) to the interrupted complex-fracture pattern (scenarios 3–4). Importantly, the 18 MPa injection-production pressure difference in Scenario 3–4 is even lower than that in scenarios 3-1, indicating acceptable injectivity and greater operational benefits. Despite slightly higher heat losses in interrupted networks (Fig. 10a), their higher production rates (Fig. 10d) and higher surface production temperatures enable them to produce more net power and further convert more electricity. Thus, interrupted vertical-fracture networks, particularly those with complex fracture configurations, present a promising approach for optimizing EGS heat recovery and electricity production.

3.4. EGS performance under different shear-fracture systems

Fig. 11 illustrates the EGS performance across models with different shear-fracture networks. The ranking of surface production temperature follows: Scenario 4-1 (207.8 °C) > Scenario 4-3 (207.2 °C) > Scenario 4-2 (206.3 °C) > Scenario 4-4 (205.4 °C). However, electricity output ranks differently: Scenario 4-3 (1136.7 GWh) > Scenario 4-1 (1134.9 GWh) > Scenario 4-4 (1120.1 GWh) > Scenario 4-2 (1114.7 GWh).

The higher surface production temperatures observed in scenarios with more shear fractures (scenarios 4-1 and 4-3) compared to those with fewer shear fractures (scenarios 4-2 and 4-2) result from the increased complexity of flow paths. A more intricate shear-fracture network provides a larger high-conductivity heat mining area, slowing the movement of cold injected fluid toward production wells. This also reduces the required injection pressure and the injection-production pressure difference (Fig. 11c), but its improved flowability causes a higher water production rate (Fig. 11d). Additionally, greater production rates reduce temperature drops and heat losses, with heat losses of −134.1 W/m and −133.8 W/m in scenarios 4-1 and 4-3, compared to −137.6 W/m and −137.8 W/m in scenarios 4-2 and 4-2. Consequently, cases with more shear fractures generate higher net power and convert more electricity due to the combined effects of elevated surface production temperature and increased water production mass rate.

Compared to lower-permeability fracture systems (scenarios 4-1/4-2), higher-permeability fracture networks (scenarios 4-3/4-4) allow cold injected fluid to reach production wells more quickly, lowering surface production temperatures. Higher permeability also enhances fluid injectivity, reducing the required injection pressure and further decreasing the injection-production pressure difference (Fig. 11c). Additionally, slightly higher water production rates are observed in the

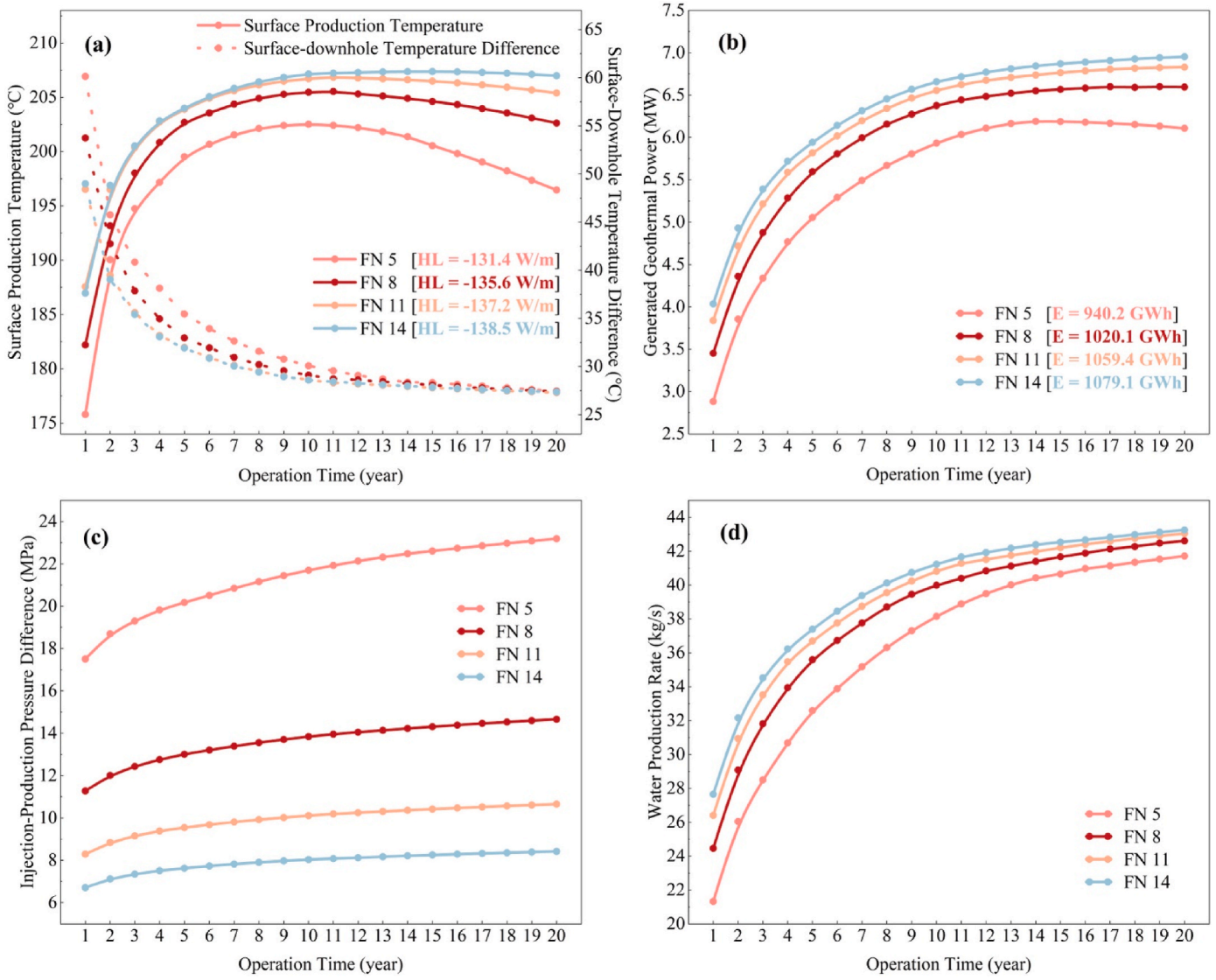

Fig. 8. EGS performance of models with different fracture numbers: (a) surface production temperature and temperature loss within wellbores; (b) geothermal power and electricity generation; (c) injection-production pressure difference; and (d) water production rate.

higher-permeability scenarios (Fig. 11d), leading to similar heat losses across these cases (Scenario 4-1: 134.1 W/m vs. Scenario 4-3: −133.8 W/m; Scenario 4-2: 137.6 W/m vs. Scenario 4-4: −137.8 W/m). As a result, higher-permeability fracture networks perform better in heat extraction compared to lower-permeability networks.

When evaluating the impact of shear fracture complexity and permeability on EGS heat mining performance, fracture complexity has a more significant influence. Specifically, tripling the number of shear fractures increases geothermal electricity generation from 1114.7 GWh to 1134.9 GWh, whereas tripling the average permeability results in a smaller increase, from 1134.9 GWh to 1136.7 GWh. Importantly, reservoirs with more shear fractures significantly improve injectivity during the fluid injection process, thereby reducing operational challenges. For example, in lower-permeability cases, increasing shear fracture number reduces the injection-production pressure difference from 34 MPa to 22 MPa, and meanwhile, in higher-permeability cases, it decreases from 32 MPa to 21 MPa. Therefore, operators should prioritize creating or connecting more pre-existing fractures during HDR stimulation to maximize heat extraction efficiency, rather than focusing on the solutions for improving fracture permeability.

4. Discussions

This study develops 3D thermal-hydraulic-mechanical-chemical (THMC) models, incorporating wellbore heat loss, to characterize heat extraction performance during EGS development. Although previous studies have widely employed multi-physics coupling to understand EGS performance, most have primarily focused on variations in underground reservoir properties during EGS operations, such as fracture aperture and matrix rock changes [47,78,79]. However, given the depth at which EGS typically operates, heat or temperature loss within wellbores is also critical to overall heat recovery. The simulations presented in this work, for the first time, not only capture variations in reservoir performance but also accurately estimate temperature losses during fluid injection and lifting within the wellbores. The results show a 9.9 %, 3.6 %, and 11.7 % difference in electricity generation when comparing the THMC model with the TH, THM, and THC models, and a 7.7 % variation in thermal power output when wellbore heat loss is included or excluded. These findings emphasize the importance of incorporating all mechanisms of heat transfer, fluid flow, mechanical deformation, chemical reactions, and wellbore heat loss in EGS assessments. Therefore, the integrated THMC and wellbore heat loss model proposed in this study offers a more comprehensive evaluation framework, enhancing the

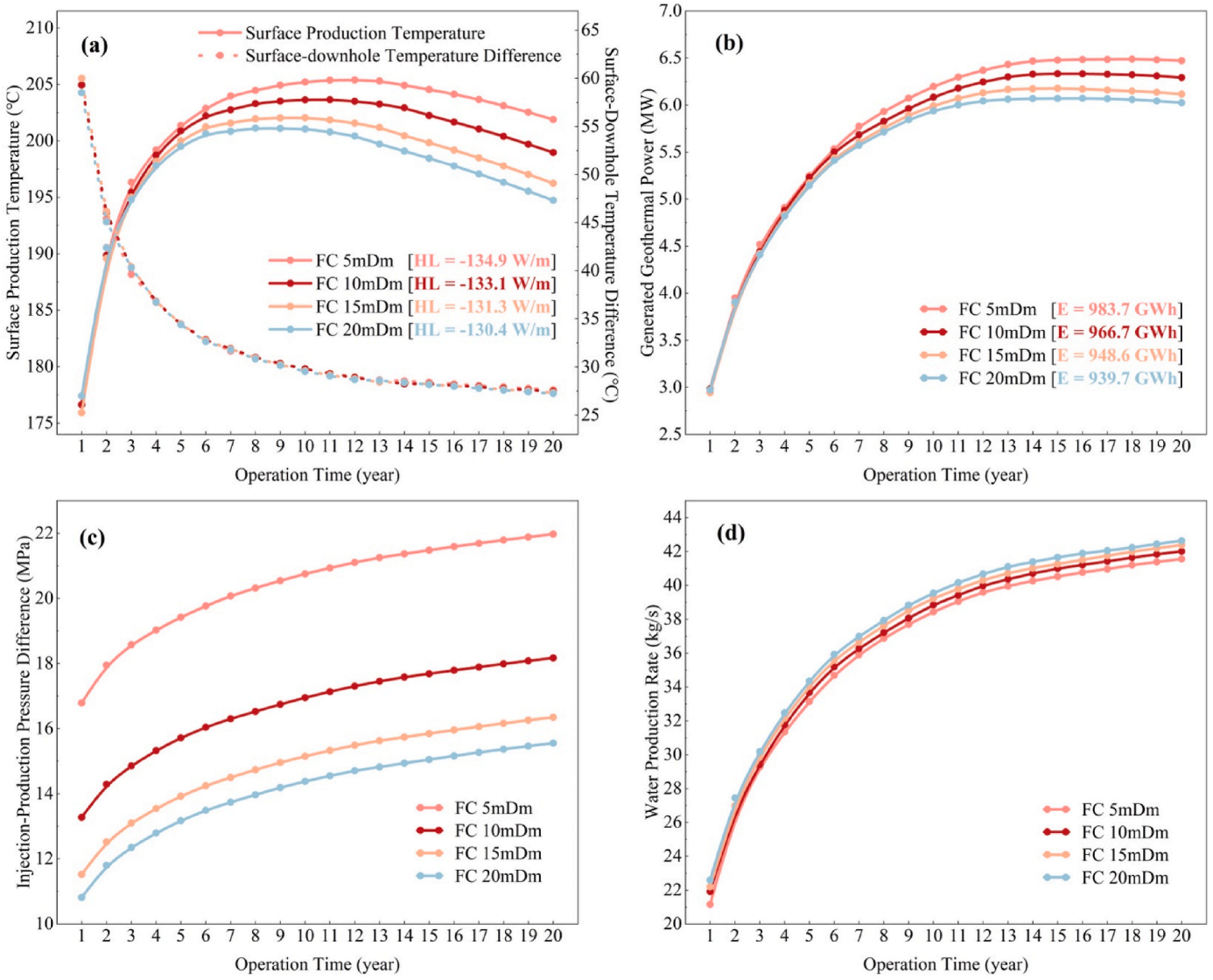

Fig. 9. EGS performance of models with different fracture conductivity: (a) surface production temperature and temperature loss within wellbores; (b) geothermal power and electricity generation; (c) injection-production pressure difference; and (d) water production rate.

understanding of EGS development performance from subsurface to surface.

In addition to the heat extraction process, HDR fracturing is also a crucial stage in EGS development. Similar to operational parameters, induced fracture patterns significantly impact heat recovery. Vertical-fracture and shear-fracture systems are two common engineered fracture networks in current EGS projects, and both have been considered in previous studies, including research on the complexity of vertical-fracture networks and the sensitivity of their properties [6]. However, without integrating subsurface multi-physics and wellbore heat loss, previous studies have lacked an accurate characterization of the entire EGS operation process. Furthermore, these two fracture systems have often been studied in isolation. While reservoir properties such as stress distribution, rock type, and natural fracture distribution play an important role in fracture propagation, vertical-fracture and shear-fracture networks can be engineered by controlling operating parameters [6]. Thus, investigating heat recovery under various fracture patterns is essential.

This study analyzes the heat recovery performance of both vertical-fracture and shear-fracture systems using the combined THMC and wellbore heat loss model. The complexity and sensitivity of these fracture networks are also explored, providing valuable insights for operators selecting effective stimulation methods during EGS development. The results show that complex vertical-fracture systems (primary fractures with branch fractures) outperform simple systems (primary fractures only) in heat recovery, and interrupted fracture networks generate more power and electricity than continuous patterns. Although interrupted fracture systems increase the injection pressure by 4 MPa during the heat transmission fluid injection process compared to continuous fracture systems, the presence of branch fractures helps mitigate this challenge. In fact, complex fracture systems show a 5 MPa reduction in injection pressure requirements compared to simple fracture systems. Therefore, operators could consider using CO_2 or other potential carriers as the fracturing fluid to stimulate HDR through both the injector and producer, creating an interrupted, complex fracture network in the reservoir. Furthermore, factors such as fracture interference, heat extraction area, and flowability significantly influence EGS performance. It should be considered to create more fractures with larger fracture spacing to reduce interference and expand the heat extraction area. However, the enhancement in heat recovery becomes less pronounced as the number of fractures and spacing increase, while technical and economic challenges rise. Thus, optimizing these factors from both technical and economic perspectives is crucial. In terms of fracture conductivity, higher conductivity causes earlier thermal

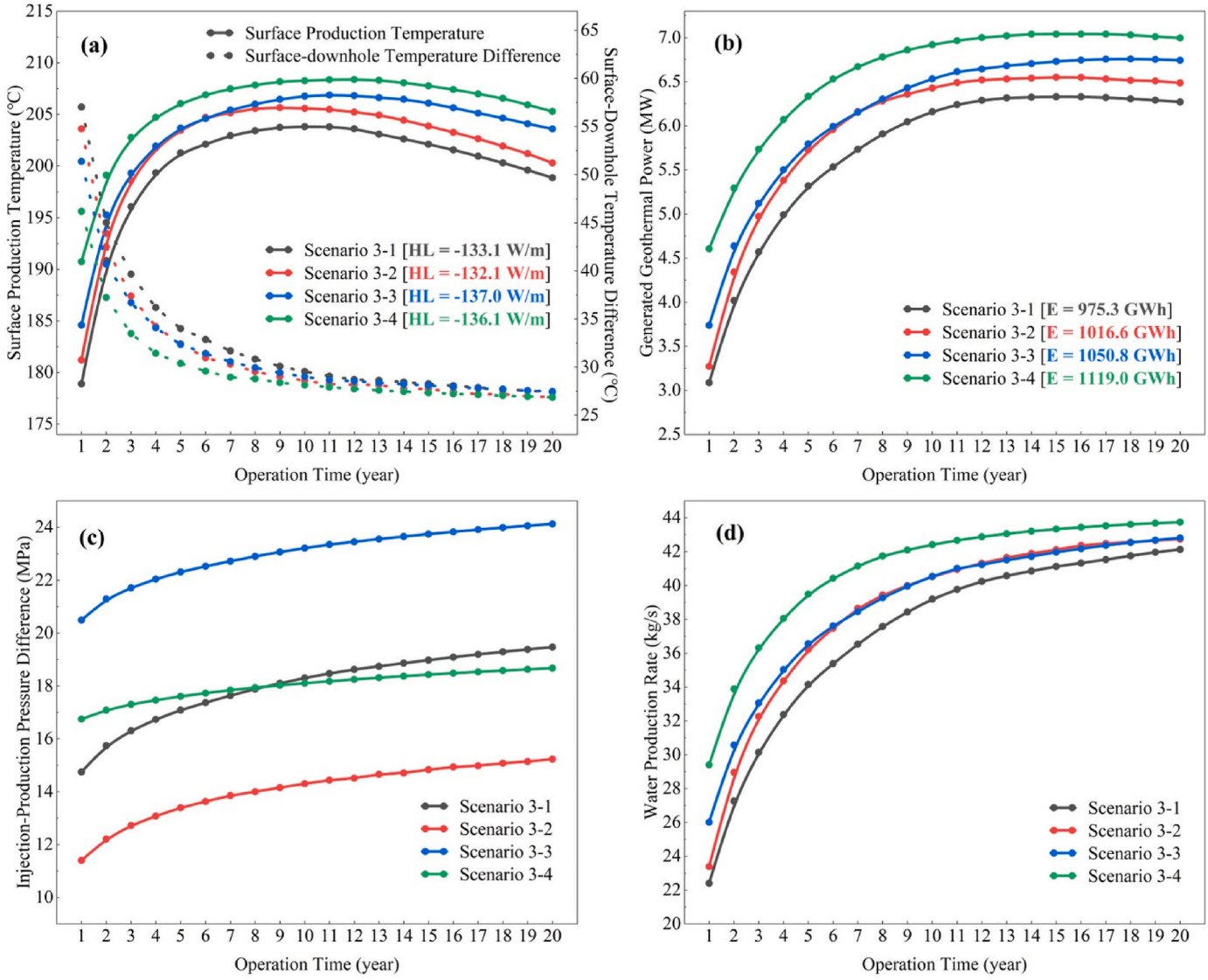

Fig. 10. EGS performance of models with different vertical-fracture networks: (a) surface production temperature and temperature loss within wellbores; (b) geothermal power and electricity generation; (c) injection-production pressure difference; and (d) water production rate.

breakthroughs and reduced heat recovery, while lower conductivity slows heat extraction, necessitating careful design of this parameter.

For shear-fracture networks, both the number and permeability of shear fracture positively influence EGS heat mining performance. However, the number of shear fractures has a more substantial impact, as tripling the number of fractures results in approximately a 2 % increase in heat recovery, whereas tripling the permeability only contributes a 0.2 % increase. Importantly, shear-fracture systems often present better heat extraction performance than the vertical-fracture networks studied, with the lowest geothermal electricity generation in shear-fracture systems only 0.4 % less than that of interrupted complex vertical-fracture networks. Although shear fracturing involves lower technical challenges such as lower treatment pressure and the lack of need for proppants [6], fewer shear fractures require a 54.7 % higher injection pressure to inject the same volume of fluid, increasing operational challenges during the heat extraction stage. Therefore, this stimulation method is particularly well-suited for reservoirs with abundant pre-existing natural fractures, where more shear fractures can be easily formed, reducing injection pressure requirements and enhancing heat recovery efficiency.

For reservoirs with limited pre-existing fractures, addressing the challenge of high injection pressure requirements during the heat extraction stage requires increasing the high-conductivity area within the reservoir by creating additional fractures. CO_2 fracturing can be particularly effective in these reservoirs, as it facilitates the development of complex fracture networks, including both primary and secondary fractures [80]. Meanwhile, fracturing both injection and production wells is recommended to establish an interrupted fracture network. In addition, a combination of hydraulic and shear fracturing techniques can be used in these reservoirs to clean and reopen natural fractures while generating new fractures that connect these reopened fractures, thereby improving the overall reservoir connectivity. Furthermore, leveraging insights from previous studies, cold fluid injection during fracturing represents another viable strategy since it can create new and/or secondary fractures due to the significant temperature difference between the fracturing fluid and the formation [6].

5. Conclusions

This study develops coupled THMC and wellbore heat loss models to evaluate EGS heat mining performance across different fracture networks. Both vertical-fracture and shear-fracture systems are analyzed, with a focus on fracture complexity and properties.

The results show that the fully coupled THMC model presents over

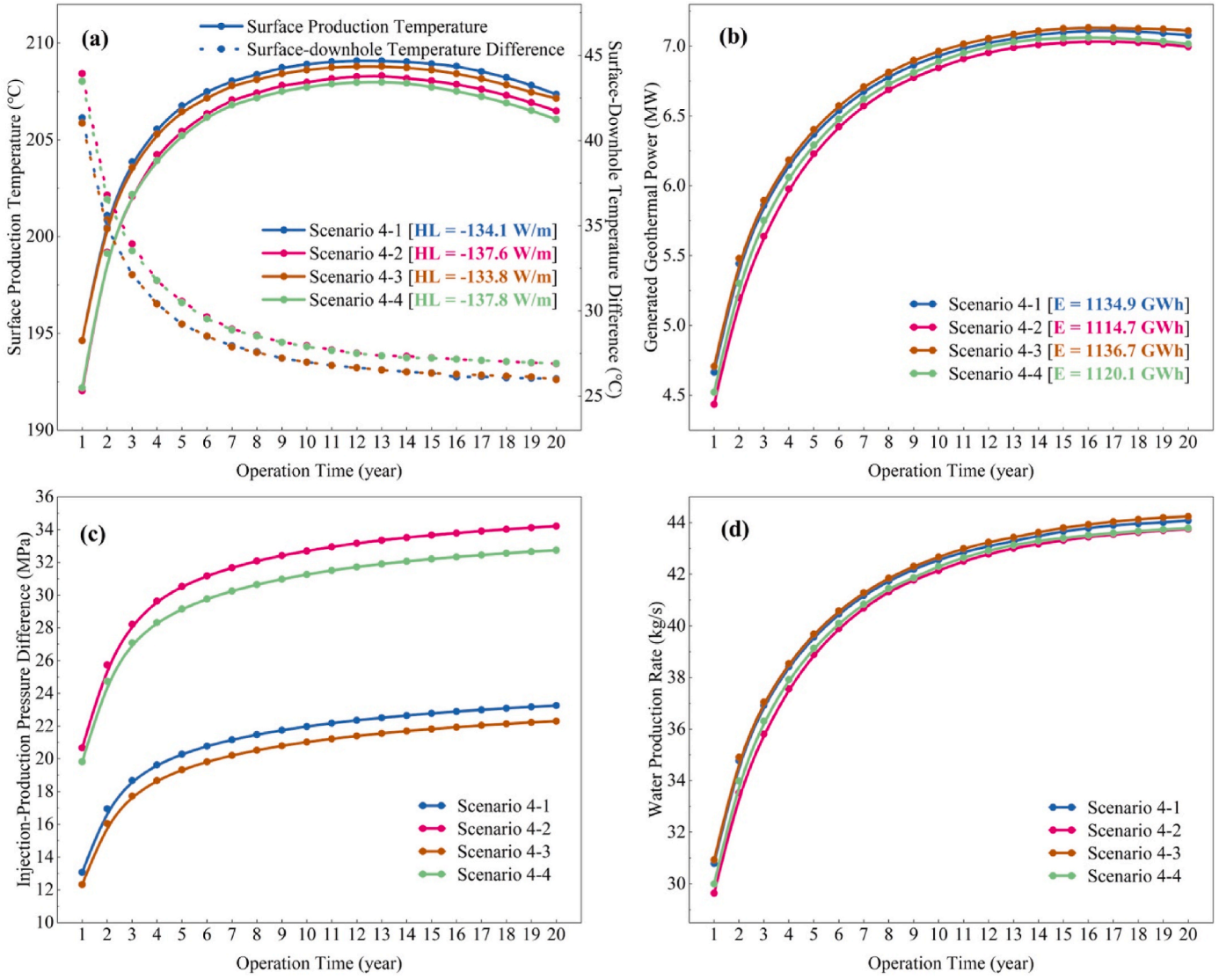

Fig. 11. EGS performance of models with different shear-fracture networks: (a) surface production temperature and temperature loss within wellbores; (b) geothermal power and electricity generation; (c) injection-production pressure difference; and (d) water production rate.

3.6 % difference in electricity generation compared to TH, THM, and THC models, with wellbore heat loss accounting for approximately 7.7 % of the thermal power recorded at the surface. This highlights the necessity of incorporating all mechanisms of heat transfer, fluid flow, mechanical deformation, chemical reactions, and wellbore heat loss in EGS assessments. Consequently, the proposed coupled models provide a more accurate characterization of EGS heat extraction performance by capturing both in-depth reservoir variations and wellbore thermal effects during fluid injection and lifting.

For different fracture properties, EGS heat recovery improves with increasing fracture spacing and number but decreases with increasing fracture conductivity. However, the electricity generation gains diminish as fracture spacing increases, dropping from 13.1 % to 2.6 % and 0.6 % at larger spacings, a trend also observed with fracture number variations. Although lower fracture conductivity enhances heat extraction in vertical-fracture systems, reducing conductivity from 20 mDm to 5 mDm increases the required injection pressure by 46.7 %, significantly improving operational challenges. Excessively low fracture conductivity can also result in ineffective fluid flow in the reservoir. Therefore, an effective design of these parameters is critical in the HDR stimulation process.

Among vertical-fracture systems, the interrupted complex fracture system achieves the highest electricity output at 1119.0 GWh. Although interrupted fractures require higher injection pressure, the complex fracture pattern effectively offsets this challenge, resulting in an injection-production pressure difference of 18 MPa, which is comparable to the 19 MPa observed in continuous simple-fracture networks. Therefore, interrupted complex fracture networks are recommended when selecting a vertical fracture network.

For shear-fracture networks, shear-fracture systems generally outperform vertical-fracture networks in heat extraction. The configuration with high permeability and a greater number of fractures produces the highest electricity output at 1136.7 GWh. Under the same parameter increase, adding more fractures contributes an additional 20.2 GWh over the operation period, whereas increasing permeability improves electricity generation by only 2.2 GWh. This indicates that fracture number has a more significant impact on EGS heat recovery than permeability. In addition, increasing fracture number results in an approximately 54.7 % rise in the injection-production pressure difference, suggesting that shear fracturing is more effective in reservoirs with abundant pre-existing natural fractures.

This work provides a comprehensive and accurate evaluation of EGS performance and offers valuable insights for HDR fracturing and heat extraction operations. However, it is limited by a limited range of

fracture networks considered. Operators still need to conduct optimization studies to determine the optimal fracturing strategy that can significantly enhance overall heat recovery. Therefore, our future research will consider more fracture networks and develop an efficient optimization tool to assist decision-making from subsurface HDR fracturing to field heat extraction operations.

CRediT authorship contribution statement

Zhenqian Xue: Conceptualization, Methodology, Software, Validation, Investigation, Data curation, Writing – original draft, Writing – review & editing. **Zichao Wei:** Data curation, Writing – review & editing. **Haoming Ma:** Investigation, Writing – review & editing. **Zhe Sun:** Validation, Writing – review & editing. **Chengang Lu:** Software, Writing – review & editing. **Zhangxin Chen:** Conceptualization, Supervision, Writing – review & editing.

Declaration of competing interest

The authors declare that they have no known competing financial interests or personal relationships that could have appeared to influence the work reported in this paper.

Acknowledgments

This research has been made possible by contributions from the Natural Sciences and Engineering Research Council (NSERC)/Energi Simulation Industrial Research Chair in Reservoir Simulation, the Alberta Innovates (iCore) Chair in Reservoir Modeling, and the Energi Simulation/Frank and Sarah Meyer Collaboration Centre.

Data availability

Data will be made available on request.

References

[1] Xue Z, Chen Z. Deep learning based production prediction for an enhanced geothermal system (EGS). In: OnePetro; 2023. https://doi.org/10.2118/212754-MS.
[2] Enhanced geothermal shot, Energy.Gov. https://www.energy.gov/eere/geothermal/enhanced-geothermal-shot (accessed October 9, 2024).
[3] Breede K, Dzebisashvili K, Liu X, Falcone G. A systematic review of enhanced (or engineered) geothermal systems: past, present and future. Geotherm Energy 2013;1:4. https://doi.org/10.1186/2195-9706-1-4.
[4] Charlez P, Lemonnier P, Ruffet C, Bouteca MJ, Tan C. Thermally induced fracturing: analysis of a field case in north sea. SPE-36916-MS, https://doi.org/10.2118/36916-MS; 1996.
[5] Turcotte DL, Schubert G. Geodynamics. Cambridge University Press; 2002.
[6] Li S, Wang S, Tang H. Stimulation mechanism and design of enhanced geothermal systems: a comprehensive review. Renew Sustain Energy Rev 2022;155:111914. https://doi.org/10.1016/j.rser.2021.111914.
[7] Song X, Guo Y, Zhang J, Sun N, Shen G, Chang X, Yu W, Tang Z, Chen W, Wei W, Wang L, Zhou J, Li X, Li X, Zhou J, Xue Z. Fracturing with carbon dioxide: from microscopic mechanism to reservoir application. Joule 2019;3:1913–26. https://doi.org/10.1016/j.joule.2019.05.004.
[8] Isaka BLA, Ranjith PG, Rathnaweera TD, Perera MSA, Kumari WGP. Influence of long-term operation of supercritical carbon dioxide based enhanced geothermal system on mineralogical and microstructurally-induced mechanical alteration of surrounding rock mass. Renew Energy 2019;136:428–41. https://doi.org/10.1016/j.renene.2018.12.104.
[9] Feng C, Wang H, Jing Z. Investigation of heat extraction with flowing CO2 from hot dry rock by numerical study. Renew Energy 2021;169:242–53. https://doi.org/10.1016/j.renene.2021.01.037.
[10] Hou L, Zhang S, Elsworth D, Liu H, Sun B, Geng X. Review of fundamental studies of CO2 fracturing: fracture propagation, propping and permeating. J Pet Sci Eng 2021;205:108823. https://doi.org/10.1016/j.petrol.2021.108823.
[11] Siratovich P, Sass I, Homuth S, Bjornsson A. Thermal stimulation of geothermal reservoirs and laboratory investigation of thermally induced fractures. Trans. - Geotherm. Resour. Counc. 2011;35:1529–35.
[12] Kelkar S, WoldeGabriel G, Rehfeldt K. Lessons learned from the pioneering hot dry rock project at fenton hill, USA. Geothermics 2016;63:5–14. https://doi.org/10.1016/j.geothermics.2015.08.008.
[13] Jung R. EGS—goodbye or back to the future. In: Isrm int. Conf. Eff. Sustain. Hydraul. Fract. ISRM; 2013. ISRM–ICHF.
[14] Evans KF, Zappone A, Kraft T, Deichmann N, Moia F. A survey of the induced seismic responses to fluid injection in geothermal and CO2 reservoirs in Europe. Geothermics 2012;41:30–54. https://doi.org/10.1016/j.geothermics.2011.08.002.
[15] Baria R, Baumgärtner J, Gérard A, Jung R, Garnish J. European HDR research programme at soultz-sous-forêts (France) 1987–1996. Geothermics 1999;28:655–69. https://doi.org/10.1016/S0375-6505(99)00036-X.
[16] McClure MW, Horne RN. An investigation of stimulation mechanisms in enhanced geothermal systems. Int J Rock Mech Min Sci 2014;72:242–60. https://doi.org/10.1016/j.ijrmms.2014.07.011.
[17] Tenma N, Yamaguchi T, Zyvoloski G. The hijiori hot dry rock test site, Japan. Geothermics 2008;37:19–52. https://doi.org/10.1016/j.geothermics.2007.11.002.
[18] H. Kaieda, S. Sasaki, D. Wyborn, Comparison of characteristics of micro-earthquakes observed during hydraulic stimulation operations in ogachi, Hijiori and cooper basin HDR projects.
[19] Pemecker G. In: Altheim geothermal plant for electricity production by ORC-turbogenerator. Peter Lang Altheim Austria: Cent. Hydrogiologie Univ. Neuchatel; 1999.
[20] Bertini G, Casini M, Gianelli G, Pandeli E. Geological structure of a long-living geothermal system, larderello, Italy. Terra Nova 2006;18:163–9.
[21] Zimmermann G, Moeck I, Blöcher G. Cyclic waterfrac stimulation to develop an enhanced geothermal system (EGS)—conceptual design and experimental results. Geothermics 2010;39:59–69. https://doi.org/10.1016/j.geothermics.2009.10.003.
[22] Cuellar G. Geothermal development in El Salvador. 1981.
[23] K.M. Kovac, J.N. Moore, S.J. Lutz, Geologic framework of the east flank, coso geothermal field: implications for EGS development.
[24] S.H. Hickman, N.C. Davatzes, In-Situ stress and fracture characterization for planning of an egs stimulation in the desert peak geothermal field, nevada.
[25] Reynolds SD, Mildren SD, Hillis RR, Meyer JJ. Constraining stress magnitudes using petroleum exploration data in the cooper–eromanga basins, Australia. Tectonophysics 2006;415:123–40. https://doi.org/10.1016/j.tecto.2005.12.005.
[26] Lu S-M. A global review of enhanced geothermal system (EGS). Renew Sustain Energy Rev 2018;81:2902–21. https://doi.org/10.1016/j.rser.2017.06.097.
[27] Bracke R, Cicr SJ, Rica C. Geothermal energy–low enthalpy technologies. In: Oral present. Present. Congr. Nac. Energ.; 2012.
[28] Zhang Y-J, Guo L-L, Li Z-W, Yu Z-W, Xu T-F, Lan C-Y. Electricity generation and heating potential from enhanced geothermal system in Songliao Basin, China: different reservoir stimulation strategies for tight rock and naturally fractured formations. Energy 2015;93:1860–85. https://doi.org/10.1016/j.energy.2015.10.059.
[29] Zimmermann G, Tischner T, Legarth B, Huenges E. Pressure-dependent production efficiency of an enhanced geothermal system (EGS): stimulation results and implications for hydraulic fracture treatments, Rock. Phys. Nat. Hazards 2009:1089–106.
[30] Geothermie st.gallen: projekt. https://www.geothermie.stadt.sg.ch/projekt.html. [Accessed 9 October 2024].
[31] J. Garcia, M. Walters, J. Beall, C. Hartline, A. Pingol, S. Pistone, K. Goyal, M. Wright, T. Conant, Overview of the northwest geysers EGS demonstration project.
[32] T.T. Cladouhos, S. Petty, Y. Nordin, M. Moore, K. Grasso, M. Uddenberg, M. Swyer, B. Julian, G. Foulger, F. Consulting, Microseismic monitoring of newberry volcano egs demonstration.
[33] Jeanne P, Rutqvist J, Dobson PF, Walters M, Hartline C, Garcia J. The impacts of mechanical stress transfers caused by hydromechanical and thermal processes on fault stability during hydraulic stimulation in a deep geothermal reservoir. Int J Rock Mech Min Sci 2014;72:149–63. https://doi.org/10.1016/j.ijrmms.2014.09.005.
[34] Beginn der stimulation im EGS-projekt newberry geothermal | informationsportal tiefe geothermie. https://www.tiefegeothermie.de/top-themen/beginn-der-stimulation-im-egs-projekt-newberry-geothermal. [Accessed 9 October 2024].
[35] Baujard C, Genter A, Dalmais E, Maurer V, Hehn R, Rosillette R, Vidal J, Schmittbuhl J. Hydrothermal characterization of wells GRT-1 and GRT-2 in rittershoffen, France: implications on the understanding of natural flow systems in the rhine graben. Geothermics 2017;65:255–68. https://doi.org/10.1016/j.geothermics.2016.11.001.
[36] H. Farndale, R. Law, An update on the united downs geothermal power project, Cornwall, UK.
[37] Eden GeoPower technology. https://www.edengeopower.com/technology. [Accessed 10 February 2025].
[38] Shi Y, Song X, Li J, Wang G, YuLong F, Geng L. Analysis for effects of complex fracture network geometries on heat extraction efficiency of a multilateral-well enhanced geothermal system. Appl Therm Eng 2019;159:113828. https://doi.org/10.1016/j.applthermaleng.2019.113828.
[39] Ma D, Duan H, Zhang Q, Zhang J, Li W, Zhou Z, Liu W. A numerical gas fracturing model of coupled thermal, flowing and mechanical effects. Comput. Mater. Contin. 2020;65:2123–41. https://doi.org/10.32604/cmc.2020.011430.
[40] Slatlem Vik H, Salimzadeh S, Nick HM. Heat recovery from multiple-fracture enhanced geothermal systems: the effect of thermoelastic fracture interactions. Renew Energy 2018;121:606–22. https://doi.org/10.1016/j.renene.2018.01.039.
[41] Aliyu MD, Archer RA. Numerical simulation of multifracture HDR geothermal reservoirs. Renew Energy 2021;164:541–55. https://doi.org/10.1016/j.renene.2020.09.085.
[42] Liu G, Yuan Z, Zhou C, Fu Z, Rao Z, Liao S. Heat extraction of enhanced geothermal system : impacts of fracture topological complexities. Appl Therm Eng 2023;219:119236. https://doi.org/10.1016/j.applthermaleng.2022.119236.
[43] Liao J, Xu B, Mehmood F, Hu K, Wang H, Hou Z, Xie Y. Numerical study of the long-term performance of EGS based on discrete fracture network with

consideration of fracture deformation. Renew Energy 2023;216:119045. https://doi.org/10.1016/j.renene.2023.119045.
[44] Li S, Feng X-T, Zhang D, Tang H. Coupled thermo-hydro-mechanical analysis of stimulation and production for fractured geothermal reservoirs. Appl Energy 2019;247:40–59. https://doi.org/10.1016/j.apenergy.2019.04.036.
[45] Salimzadeh S, Nick HM. A coupled model for reactive flow through deformable fractures in Enhanced Geothermal Systems. Geothermics 2019;81:88–100. https://doi.org/10.1016/j.geothermics.2019.04.010.
[46] Chen S, Ding B, Gong L, Huang Z, Yu B, Sun S. Comparison of multi-field coupling numerical simulation in hot dry rock thermal exploitation of enhanced geothermal systems. Adv. Geo-Energy Res. 2019;3:396–409. https://doi.org/10.26804/ager.2019.04.07.
[47] Song G, Song X, Xu F, Li G, Shi Y, Ji J. Contributions of thermo-poroelastic and chemical effects to the production of enhanced geothermal system based on thermo-hydro-mechanical-chemical modeling. J Clean Prod 2022;377:134471. https://doi.org/10.1016/j.jclepro.2022.134471.
[48] Gao X, Qiao Y, Wang Z, Li T. Production potential assessment of enhanced geothermal system with thermos-hydraulic-mechanical-chemical mechanism in hot dry rock. Energy Convers Manag 2024;309:118410. https://doi.org/10.1016/j.enconman.2024.118410.
[49] Zhang W, Han D, Wang B, Chen Y, Jiao K, Gong L, Yu B. Thermal-hydraulic-mechanical-chemical modeling and simulation of an enhanced geothermal system based on the framework of extended finite element methods - embedded discrete fracture model. J Clean Prod 2023;415:137630. https://doi.org/10.1016/j.jclepro.2023.137630.
[50] Rathnaweera TD, Wu W, Ji Y, Gamage RP. Understanding injection-induced seismicity in enhanced geothermal systems: from the coupled thermo-hydro-mechanical-chemical process to anthropogenic earthquake prediction. Earth Sci Rev 2020;205:103182. https://doi.org/10.1016/j.earscirev.2020.103182.
[51] Xu H, Liu G, Zhao Z, Ma F, Wang G, Chen Y. Coupled THMC modeling on chemical stimulation in fractured geothermal reservoirs. Geothermics 2024;116:102854. https://doi.org/10.1016/j.geothermics.2023.102854.
[52] Shi H, Holmes JA, Durlofsky LJ, Aziz K, Diaz LR, Alkaya B, Oddie G. Drift-flux modeling of two-phase flow in wellbores. SPE J 2005;10:24–33. https://doi.org/10.2118/84228-PA.
[53] Ramey HJ. Wellbore heat transmission. J. Pet. Technol. 1962;14:427–35. https://doi.org/10.2118/96-PA.
[54] Brown CS, Falcone G. Investigating heat transmission in a wellbore for Low-Temperature, Open-Loop geothermal systems. Therm Sci Eng Prog 2024;48:102352. https://doi.org/10.1016/j.tsep.2023.102352.
[55] Z. Xue, H. Ma, Z. Chen, Numerical investigation of energy production from an enhanced geothermal system associated with CO2 geological sequestration, in: OnePetro, n.d.
[56] Xue Z, Zhang Y, Ma H, Lu Y, Zhang K, Wei Y, Yang S, Wang M, Chai M, Sun Z, Deng P, Chen Z. A combined neural network forecasting approach for CO2-enhanced shale gas recovery. SPE J 2024;29:4459–70. https://doi.org/10.2118/219774-PA.
[57] Ma H, Yang Y, Zhang Y, Li Z, Zhang K, Xue Z, Zhan J, Chen Z. Optimized schemes of enhanced shale gas recovery by CO2-N2 mixtures associated with CO2 sequestration. Energy Convers Manag 2022;268:116062. https://doi.org/10.1016/j.enconman.2022.116062.
[58] Lei Z, Zhang Y, Zhang S, Fu L, Hu Z, Yu Z, Li L, Zhou J. Electricity generation from a three-horizontal-well enhanced geothermal system in the Qiabuqia geothermal field, China: slickwater fracturing treatments for different reservoir scenarios. Renew Energy 2020;145:65–83. https://doi.org/10.1016/j.renene.2019.06.024.
[59] Kim SJ, Kim D, Lee DY. On the local thermal equilibrium in microchannel heat sinks. Int. J. Heat Mass Transf. 2000;43:1735–48. https://doi.org/10.1016/S0017-9310(99)00259-8.
[60] Pandey SN, Chaudhuri A, Rajaram H, Kelkar S. Fracture transmissivity evolution due to silica dissolution/precipitation during geothermal heat extraction. Geothermics 2015;57:111–26. https://doi.org/10.1016/j.geothermics.2015.06.011.
[61] Chen Z. Reservoir simulation: mathematical techniques in oil recovery. SIAM; 2007.
[62] Guo T, Gong F, Wang X, Lin Q, Qu Z, Zhang W. Performance of enhanced geothermal system (EGS) in fractured geothermal reservoirs with CO2 as working fluid. Appl Therm Eng 2019;152:215–30. https://doi.org/10.1016/j.applthermaleng.2019.02.024.
[63] Guo T, Tang S, Sun J, Gong F, Liu X, Qu Z, Zhang W. A coupled thermal-hydraulic-mechanical modeling and evaluation of geothermal extraction in the enhanced geothermal system based on analytic hierarchy process and fuzzy comprehensive evaluation. Appl Energy 2020;258:113981. https://doi.org/10.1016/j.apenergy.2019.113981.
[64] Lasaga AC. Chemical kinetics of water-rock interactions. https://click.endnote.com/viewer?doi=10.1029%2Fjb089ib06p04009&token=WzM4NjkwOTksIjEwLjEwMjkvamIwODlpYjA2cDA0MDA5Il0.dsHhN1Hm7mVPDqq9YKNJd6xsO3U. [Accessed 25 September 2024].
[65] Yasuhara H, Kinoshita N, Ogata S, Cheon D-S, Kishida K. Coupled thermo-hydro-mechanical-chemical modeling by incorporating pressure solution for estimating the evolution of rock permeability. Int J Rock Mech Min Sci 2016;86:104–14. https://doi.org/10.1016/j.ijrmms.2016.03.015.
[66] D. Tran, New iterative coupling between a reservoir simulator and a geomechanics module.
[67] Bahonar M, Azaiez J, Chen Z. Two issues in wellbore heat flow modelling along with the prediction of casing temperature in steam injection wells. J Can Pet Technol 2011;50(01):43–63.
[68] Xue Z, Yao S, Ma H, Zhang C, Zhang K, Chen Z. Thermo-economic optimization of an enhanced geothermal system (EGS) based on machine learning and differential evolution algorithms. Fuel 2023;340:127569. https://doi.org/10.1016/j.fuel.2023.127569.
[69] Xue Z, Zhang K, Zhang C, Ma H, Chen Z. Comparative data-driven enhanced geothermal systems forecasting models: a case study of Qiabuqia field in China. Energy 2023;280:128255. https://doi.org/10.1016/j.energy.2023.128255.
[70] Lei Z, Zhang Y, Yu Z, Hu Z, Li L, Zhang S, Fu L, Zhou L, Xie Y. Exploratory research into the enhanced geothermal system power generation project: the Qiabuqia geothermal field, Northwest China. Renew Energy 2019;139:52–70. https://doi.org/10.1016/j.renene.2019.01.088.
[71] Zhang C, Jiang G, Jia X, Li S, Zhang S, Hu D, Hu S, Wang Y. Parametric study of the production performance of an enhanced geothermal system: a case study at the Qiabuqia geothermal area, northeast Tibetan plateau. Renew Energy 2019;132:959–78. https://doi.org/10.1016/j.renene.2018.08.061.
[72] Chong Q, Wang J, Gates ID. Evaluation of energy extraction from a geothermal resource in central Alberta, Canada using different well configurations. Geothermics 2021;96:102222. https://doi.org/10.1016/j.geothermics.2021.102222.
[73] Song G, Song X, Li G, Xu R, Cao W, Zhao C. Multi-objective optimization of geothermal extraction from the enhanced geothermal system in Qiabuqia geothermal field, gonghe basin. Acta Geol. Sin. - Engl. Ed. 2021;95:1844–56. https://doi.org/10.1111/1755-6724.14875.
[74] Xue Z. Machine learning based techno-economic assessment and optimization of an enhanced geothermal system, Mach. Learn 2024;2024:6–21.
[75] Xue Y, Liu S, Chai J, Liu J, Ranjith PG, Cai C, Gao F, Bai X. Effect of water-cooling shock on fracture initiation and morphology of high-temperature granite: application of hydraulic fracturing to enhanced geothermal systems. Appl Energy 2023;337:120858. https://doi.org/10.1016/j.apenergy.2023.120858.
[76] Xue Z, Ma H, Sun Z, Lu C, Chen Z. Technical analysis of a novel economically mixed CO2-Water enhanced geothermal system. J Clean Prod 2024;448:141749. https://doi.org/10.1016/j.jclepro.2024.141749.
[77] Xie J, Tonkin R, Yeh A, Wang J, O'Sullivan M. Application of a geothermal wellbore simulator in evaluating an enhanced geothermal system. Geothermics 2025;125:103160. https://doi.org/10.1016/j.geothermics.2024.103160.
[78] Aliyu MD, Archer RA. A thermo-hydro-mechanical model of a hot dry rock geothermal reservoir. Renew Energy 2021;176:475–93. https://doi.org/10.1016/j.renene.2021.05.070.
[79] Cui X, Wong LNY. A 3D thermo-hydro-mechanical coupling model for enhanced geothermal systems. Int J Rock Mech Min Sci 2021;143:104744. https://doi.org/10.1016/j.ijrmms.2021.104744.
[80] Feng Y, Firoozabadi A. Phase-field simulation of hydraulic fracturing by CO2 and water with consideration of thermoporoelasticity. Rock Mech Rock Eng 2023;56:7333–55. https://doi.org/10.1007/s00603-023-03355-7.